



Micromachined Optical Fiber Sensors for Biomedical Applications

Chen Zhu, Rex E. Gerald II, and Jie Huang

Abstract

Optical fibers revolutionized the rate of information reception and transmission in telecommunications. The revolution has now extended to the field of physicochemical sensing. Optical fiber sensors (OFSs) have found a multitude of applications, spanning from structural health monitoring to biomedical and clinical measurements due to their unique physical and functional advantages, such as small dimensions, light weight, immunity to electromagnetic interference, high sensitivity and resolution, multiplexing, and remote operation. OFSs generally rely on the detection of measurand-induced changes in the optical properties of the light propagating in the fiber, where the OFS essentially functions as the conduit and physical link between the probing light waves and the physicochemical parameters under investigation. Several advanced micromachining techniques have been developed to optimize the structure of OFSs, thus improving their sensing performance. These techniques include fusion splicing, tapering, polishing, and more complicated femtosecond laser micromachining methods. This chapter discusses and reviews the most recent developments in micromachined OFSs specifically for biomedical applications. Step-by-step procedures for several optical fiber micromachining techniques are detailed.

Key words Optical fiber sensors, Micromachining, Biomedical, Biomechanical, Healthcare, Biosensors

1 Introduction

The fiber optic field has attracted extensive interest and undergone tremendous growth and advancement since the first realization of optical fibers as a telecommunication medium by C. Kao in 1960 [1]. The rapid development of optical fibers has led to the emergence of various high-quality, miniaturized, and affordable optoelectronic components and devices, resulting in numerous ideas for practical implementations using optical fibers, ranging from high-speed, long-haul, and large-capacity telecommunications, optical imaging to high-power light delivery. Optical fibers have also found applications in the sensing field because of their unique properties, such as small dimensions, light weight, immunity to electromagnetic interference (EMI), and low-transmission loss [2].

Optical fiber sensors (OFSs) have been widely and successfully used in an expansive range of sensing applications, such as structural health monitoring, down-hole monitoring, chemical and biological sensing, medical imaging, and environmental monitoring for the past four decades [3]. OFSs provide a convenient way of implementing optical sensing using integrated optics, simply by the direction of light to and collection of light from the regions under investigation via optical fibers. The OFS for biomedical applications was initially introduced in the field of endoscopy in the 1960s; to date, the endoscope has been the most successful biomedical application of OFSs [4]. In an optical fiber endoscope device, a fiber bundle is used for observing and imaging internal organs, where a portion of the fibers is used as the illumination fiber and the others are used to collect the images. The use of optical fibers enables the fabrication of an extremely compact endoscopic device with excellent flexibility and robustness, making it possible to observe and image internal orifices of the human body that are otherwise inaccessible. Due to the advancement of optical fiber sensing technology, the scope of OFSs for biomedical applications has expanded greatly to include measurements of a broad variety of physiological, chemical, and biological parameters [5]. Compared to conventional sensors employed in biomedical applications, which are based on solid-state sensing technologies (e.g., piezoresistive effect), biomedical OFSs offer outstanding advantages, including miniaturization, low cost, insensitivity to magnetic fields, chemical and corrosive inertness, biocompatibility, non-conductive, and the ability for remote operation. An obvious example is the applications of OFSs in magnetic resonance imaging (MRI) environments or in RF radiation treatment, where high magnetic/electric interferences exist, making it challenging for conventional transducers due to the metallic wires used for power and communications [6]. Additionally, the unique features of optical fibers for carrying information provide the possibility of integrating multiples sensors with diverse measurement capabilities into a single fiber, a task not possible using traditional electrical devices.

Generally, an OFS functions as the light transducer between physicochemical parameters of the investigated environment and light conduction in the OFS. The choice of a proper OFS for a specific biomedical application is dictated by both technological and practical issues, such as desired sampling volume, detection accuracy and limit, (non)invasiveness, environmental interference, which impose unique biomedical engineering challenges on fiber optic researchers [7]. Therefore, substantial caution should be used in the design and fabrication of OFSs with optimized structures and performance metrics for biomedical applications. Special requirements of the optical fiber components are diverse for the construction of different OFSs for specific applications. Taking advantage of the micromachining techniques, OFSs with various structures and

measuring performances are possible. The most commonly used micromachining process used in OFS fabrication is fusion splicing, where two pieces of optical fiber having identical or dissimilar properties are spliced together (e.g., single-mode fiber fused to a hollow-core fiber) [8]. The angle of cleavage of an optical fiber is also an important choice in the process of preparation for fusion splicing. Tapering and polishing of optical fibers are widely used for fabricating OFSs. Tapering is usually employed in developing microfibers or nanofibers which are used for ultra-sensitive chemical sensing [9]. Polishing is a versatile technique to remove a certain portion of an optical fiber to form special structures, for example, D-shaped/side-polished optical fibers [10]. On the other hand, by polishing a fiber endface to a selected angle, the light output from the optical fiber can be guided in a specific direction, which is desirable in biomedical applications, e.g., endoscope-internal imaging. In very recent years, with the advancement of laser techniques, femtosecond laser micromachining has been widely used for processing of transparent materials (e.g., glass) [11]. Different functional photonic micro/nano-structures have been successfully fabricated by micromachining methods applied to different substrates for a variety of applications, including sensing. Combining the one-step fabrication techniques enabled by femtosecond laser micromachining and the unique advantages of OFSs opens new avenues for developing a new generation of assembly-free OFSs with enhanced robustness, flexibility, and functionality.

In this chapter, we introduce micromachined optical fiber sensors for biomedical applications, including traditional methods of micromachining and more advanced ultrafast laser micromachining. The most recent developments in this field are reviewed.

Our review criteria were established to cover most of the recent advancements in micromachined OFSs for biomedical applications. Due to the rapid growth and development of micromachining methodologies and optical fiber sensing technologies, the majority of recently reported OFSs utilized one or more micromachining techniques during fabrication processes. However, most of these advanced sensors have not been demonstrated for *in vivo* clinical measurements, but they offer unparalleled advantages compared to conventional OFSs and they have huge potential to be further explored for real-world biomedical applications. Therefore, our review focuses on a basic introduction to the most recent developments in micromachining-assisted OFSs and their potential applications in biomedicine. Various optical fiber sensing techniques are discussed in detail for each specific measurand (e.g., temperature, pressure, biomarker) in clinical settings. Moreover, a few typical examples of sensing technique configurations are included for the reader's edification. The protocols for the optical fiber micromachining methods described in this chapter are based on the authors' years of experience in the optical fiber sensor arena and might vary

due to the rapid development and advancement of micromachining technologies.

The past two decades have witnessed the rapid growth of OFSs in biomedical applications. The light propagating capabilities and high flexibility of optical fibers attracted the first application of optical fibers in clinical settings for endoscopy in the 1960s. The emergence of the optical fiber imaging endoscope has enabled internal body observation and imaging, making possible the rapid determination of the presence of tumors, damaged or diseased tissue, and internal bleeding in organs. Since the 1960s, optical fibers and OFS have attracted significant attention from the health-care industry. Besides the traditional endoscope probes, more advanced imaging techniques based on optical fibers have been developed, such as optical coherence tomography (OCT) and photoacoustic imaging, where under-skin and internal scanning can be made noninvasive. Another advanced area of optical fiber used in biomedical applications is optical fiber-based biosensors, including physical and biochemical OFSs. For instance, measurements of a broad variety of different physiological parameters such as blood flow, heart rate, respiration, temperature, pressure are enabled by physical OFSs; biochemical OFSs are employed to identify and quantify particular chemical compounds and metabolic variables, such as pH, blood oxygen, glucose or to measure specific biological species (e.g., biomarkers) for diagnostic purposes. This section will introduce the most recent developments in optical fiber biosensors for biomedical applications. Particularly, optical fiber biosensors fabricated by one or more micromachining processes discussed in Subheading 3 will be mainly focused on.

1.1 Temperature Sensors

Temperature is an essential and routinely monitored physiological parameter in biomedical environments, such as in operating rooms, therapeutic rooms, and intensive care units. For instance, in recent years, minimally invasive thermal treatments, such as high-intensity focused ultrasound ablation, radiofrequency/microwave ablation, laser ablation, and cryo-ablation, have become an effective and efficient way of localized tumor removal [12]. Accurate and real-time measurements of tissue temperatures can provide a clear end-point for completing tumor ablation. Among a variety of thermometric techniques used in biomedicine (e.g., thermocouples, thermistors), optical fiber thermometers are particularly suitable due to their unique features. Optical fiber thermometers are especially attractive in temperature measurements where immunity to electromagnetic interferences are required (e.g., in MRI).

Optical fiber temperature sensors rely on a variety of transduction principles, such as temperature-dependent fluorescence, the thermal-optic effect, and thermal expansion. Taking advantage of micromachining techniques, a variety of OFS thermometers have been proposed and demonstrated. One of the most widely investigated types of OFS thermometers is based on optical interference,

and embodiments include the Fabry–Perot interferometer (FPI), the Mach–Zehnder/Michelson interferometer (MZI/MI), the Sagnac interferometer, and the multimodal interferometer [13]. These interference-based OFSs are generally modified using a micromachining process that results in excitation of multi-path light beams. The optical path difference (OPD) of the light beams varies under the influence of temperature changes due to thermal expansion and/or the thermal-optic effect. Fusion splicing and femtosecond laser micromachining are versatile techniques used to fabricate these OFSs. A section of a special optical fiber (e.g., PCF or multimode fiber) was fusion spliced between two SMFs to form an FPI device or multimodal interferometer for temperature measurements [14, 15]. A refractive-index-modified dot fabricated in an SMF by a femtosecond laser together with the fiber-optic endface was demonstrated as an FPI for temperature sensing [16]. A miniaturized concave-shaped FPI ($<100\ \mu\text{m}$) was reported for high-temperature applications fabricated by an advanced fusion splicing process [17]. Fiber-in-line MZIs fabricated by femtosecond laser micromachining were also demonstrated for measuring temperature, where a pair of microstructure were typically fabricated as the cladding mode exciter and combiner [18–21]. The thermal sensitivity of fiber Bragg grating (FBG) has also been exploited for medical applications [22]. An FBG is fabricated by introducing a periodic change in the index of refraction (i.e., Bragg grating) along a fiber core length by using a phase mask and a UV laser irradiation technique or by a femtosecond laser point-by-point (or plane-by-plane) micromachining. By tracking the shift of the Bragg wavelength of the FBG, the temperature variations can be determined [23]. Typically, these all-silica-fiber temperature sensors can function in a wide range of temperature environments, e.g., from -200 to $1000\ ^\circ\text{C}$ due to the thermal stability of fused silica with satisfactory measurement resolution (e.g., $\pm 0.5\ ^\circ\text{C}$). However, the temperature sensitivities of these sensors are not high enough due to the small coefficient of thermal expansion (CTE, $\sim 5 \times 10^{-7}/^\circ\text{C}$) and low thermal-optical coefficient (TOE, $\sim 8.3 \times 10^{-6}/^\circ\text{C}$) of silica. A promising solution to this issue is infiltrating liquid (e.g., liquid polymer, alcohol) with large TOE ($>10^{-4}/^\circ\text{C}$) into holey fibers through the microholes which can be fabricated by femtosecond laser micromachining, and using the liquid-filled fibers as the building blocks for developing temperature sensors [24–27]. Typically, the sensitivity could be enhanced by approximate three orders of magnitude, although the dynamic range is limited to tens of degrees (e.g., $20\text{--}80\ ^\circ\text{C}$), which is good enough for most biomedical applications. Besides direct thermal measurements of bodies, a temperature OFS was also designed as a respiration sensor in an MRI system by measuring the temperature variations of airflow in exhaled air [28].

Microfibers enabled by tapering micromachining technique was also explored for developing temperature sensors, where microfibers with a reduced diameter (e.g., 1–50 μm) were used as the platform for the construction of the sensors [9]. Various interferometers were micromachined in microfibers, such as an MZI and an FPI [29, 30]. Microfiber-based Bragg gratings (MFBGs) have also been demonstrated for temperature sensing [31]. The EW in a tapered fiber is greatly enhanced due to the reduced diameter in the taper waist and is sensitive to the refractive index of the surroundings around the tapered region. Therefore, coating the microfiber sensors with materials having large TOC in the tapered region can dramatically enhance the temperature sensitivity of the microfiber [32, 33]. Compared with telecommunication optical fiber-based OFSs (i.e., fibers with a diameter of 125 μm), microfiber-based OFSs provide extreme compactness and faster response time. However, microfiber-based OFSs are generally fragile and require careful packaging for practical applications.

In addition to these point temperature sensors, OFSs also offer a prospect for multiplexed or fully distributed temperature sensing based on FBGs, scattering (Raman scattering, Rayleigh scattering, and Brillouin scattering), or cascaded fiber-in-line reflectors [34–39], allowing for mapping of temperature in the area of interest during medical treatment with high spatial resolution [40–42]. For example, the temperature distribution inside a liver tissue during an RF ablation procedure was successfully measured using a device predicated on Rayleigh scattering based optical frequency domain reflectometry (OFDR, Luna OBR4600) [40]. In real-time thermal mapping, the OFDR setup was configured with a spatial resolution of 200 μm for the entire optical fiber (<20 m), an update rate of 1 Hz, and an accuracy of 0.5 $^{\circ}\text{C}$. The evolution of the spatial and temporal temperature changes in the liver tissue during RF ablation measured by the OFDR system was smooth and consistent with the anticipated physical effects. In turn, the distributed thermal mapping capability could be employed for the investigation of the fundamental physics of RF ablation and the corroboration of theoretical models.

1.2 Pressure Sensors

Pressure measurements in biomedical applications can be generally divided into two categories: monitoring isotropic pressure, such as intracranial and cardiovascular blood/fluid pressure monitoring, and sensing contact pressure, such as intervertebral pressure, force, and tactile sensing [43].

Fluid pressure measurements rely on monitoring the movement or deflection of a membrane under the influence of pressure. Intensity-modulated OFSs were originally demonstrated for measuring pressures in biomedical settings in the 1960s, where a movable reflectance membrane is interfaced with an optical fiber tip such that the intensity of light reflected and coupled into the

receiving fiber is modulated by pressure [44]. The applications of these intensity-modulated sensors are inevitably limited due to the drawback that the output signal can be modulated by a wide range of perturbations, such as the light source fluctuation and changes in reflectivity of the membrane due to oxidation. FPI is an excellent candidate for pressure measurements which offers the highest sensitivity and can be designed and implemented with great flexibility. Initially, a Fabry–Perot cavity is bonded to an optical fiber tip in an extrinsic configuration, where the pressure-sensitive diaphragm is larger in diameter than that of an optical fiber (125 μm) (which might raise a concern regarding further miniaturization) [45]. More recently, with the implementation of micromachining techniques, a new generation of miniaturized fiber-in-line FPI pressure sensors have been proposed, where the pressure-sensitive diaphragm is designed to be part of the optical fiber with the same diameter [46–48]. In these miniaturized FPI pressure sensors, typically, a hollow-core fiber is first fusion spliced onto a cleaved endface of an SMF, and the other end of the hollow core fiber is cut off using a fiber cleaver under microscope where the length of the residual hollow core fiber can be precisely controlled. Subsequently, a thin diaphragm is bonded to the open end of the hollow core fiber to form a hermetic cavity, serving as the pressure sensing element, as schematically illustrated in Fig. 1. The diaphragm deflects under pressure, which can be accurately captured by the Fabry–Perot interference that occurs between the optical fiber endface and the diaphragm. Several materials were explored as the diaphragm for highly sensitive pressure measurements, such as a polymer–metal composite film [46], a graphene layer [47], and a nano-silver film [48]. However, the structural robustness and temperature stability of these pressure sensors are poor, which hinders their way forward for practical applications, especially in harsh environments. On the other hand, all-silica FPI pressure sensors were also developed as an alternative where harsh environments are involved. Several micromachining techniques were employed for fabricating all-silica pressure sensors. A series of all-silica FPI pressure sensors were successfully fabricated using the traditional splicing-and-cutting method, followed by polishing or HF etching to further reduce the thickness of the silica diaphragm, thereby improving the pressure sensitivity [49–53]. Alternatively, femtosecond laser micromachining and advanced fusion splicing are also employed to reduce the thickness of the diaphragm to avoid using hazardous chemical etching [54–57]. The method of femtosecond laser micromachining not only reduces the thickness of the silica diaphragm but also roughens one side to eliminate the additional reflections from the outer surface of the diaphragm (i.e., reduced parasitic interferences). Electric arc discharge techniques enabled by commercial fusion splicers are a more cost-effective way for thinning a diaphragm, where the thickness of the diaphragm can be reduced

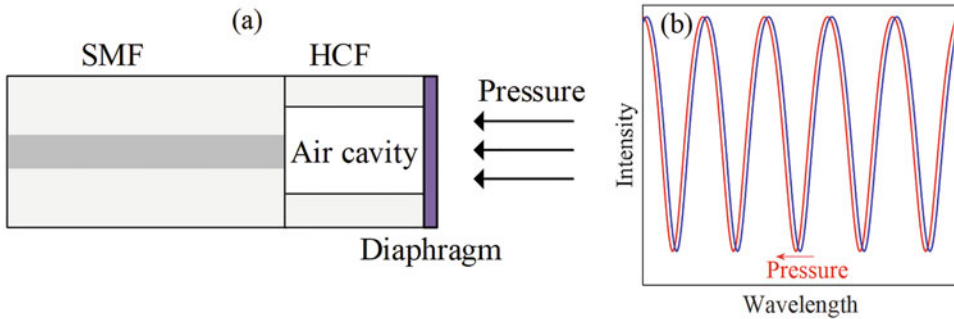


Fig. 1 Schematic of a typical diaphragm-based optical fiber FPI pressure sensor. **(a)** Schematic illustration of the sensor structure. **(b)** Response of the sensor to an increase in pressure, i.e., a shift in the reflection spectrum. As the applied pressure increases, the diaphragm deflects, resulting in a decrease in the cavity length (i.e., the distance between the optical fiber endface and the diaphragm) and thus a blue-shift of the reflection spectrum

down to 170 nm [57]. The all-silica FPI pressure sensors fabricated with advanced micromachining techniques possess excellent mechanical and temperature stability and are more biocompatible and chemically resistive than metal-diaphragm-based pressure sensors. Most of these advanced sensors were only validated in the laboratory, while biomechanical and biomedical applications have not been demonstrated yet using these sensors.

The FBG is the most widely used OFSs for contact pressure measurements in the field of biomechanics and rehabilitation applications, where FBGs could be used for detecting stress in bones and intervertebral discs, pressure distribution in orthopedic joints and human-machine interfaces (HMIs), and forces induced by tendons and ligaments [58]. In minimally invasive surgery (MIS), haptic perception is of significant importance because it enables the surgeon to feel organic tissue hardness, measure tissue properties, and evaluate the anatomical structure and, therefore, allows the surgeon to commit appropriate force control actions for tissue manipulations [59]. The high sensitivity, flexibility, and capability of multiplexing make FBGs an outstanding candidate for single-point and multi-point tactile sensing [60]. Recently, an OFS-based technique was employed to address a common problem in medical procedures, recognized as a medical device-related pressure ulcer, where a polymer patch-embedded FBG was used to measure the contact pressure between a medical device and the tissue [61]. FBG-assisted bandaging was reported for in vivo observation of the sub-bandage pressure during compression therapy, where two arrays of FBGs were entwined in a double helix form with contact-force sensitivity and immunity to temperature variations, as shown in Fig. 2 [62]. In addition to FBGs, FPIs have also been demonstrated as a promising configuration for contact pressure measurements. A miniaturized optical fiber tactile sensor based on an FPI structure was reported

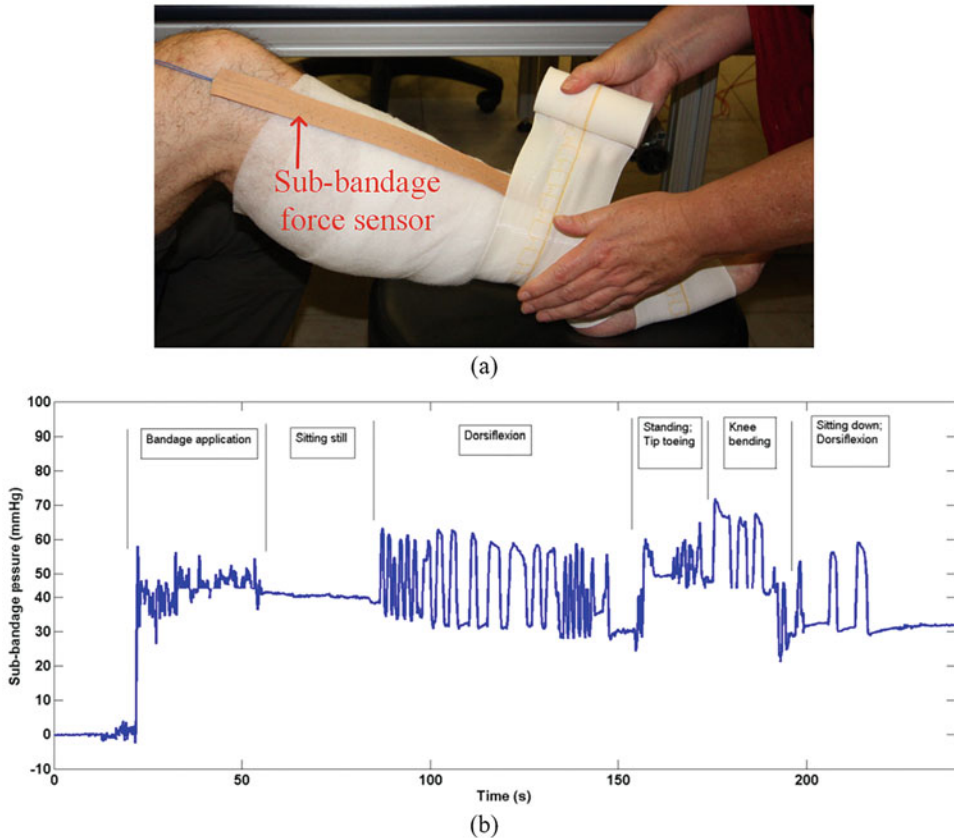


Fig. 2 An FBG-based sub-bandage force sensor [62]. (a) In vivo sub-bandage pressure measurement sensor for monitoring a wounded leg. (b) Pressure measurements at the medical gaiter during simple movements

for high-resolution needle insertion force sensing in high-field MRI environments [63]. The miniaturized optical fiber force sensor was integrated into an MRI compatible piezoelectric actuated robot for prostate brachytherapy applications [64]. Another optical fiber force sensor was reported for vitreoretinal surgery applications, where a surgical tool was integrated with a miniaturized OFS [65]. The prototype device with an outer diameter smaller than 1 mm was demonstrated for simultaneously measuring axial and lateral forces. In these FPI-based tactile sensors, an extrinsic structure was employed. Further trends should include the advanced miniaturized fiber-line structure-based OFSs for force sensing in biomedical applications. On the other hand, a Rayleigh scattering-based OFDR system was also employed for tactile sensing where the sensing SMF is embedded in a soft prosthetic forefinger [66]. The strain distribution along the forefinger was precisely mapped with high spatial resolution (~ 3 mm), opening a new possibility for perceptive soft robots.

1.3 Respiratory, Heart Rate, and Blood Flow Sensors

Respiratory and heart rates are two vital signs of the human body that are monitored online during medical examinations and procedures. Typically, the respiratory and heart rate OFSs are configured as strain sensors, which are capable of measuring the periodic mechanical movement of the chest wall (i.e., contractions and expansions) induced by breathing or cardiac activities. Sensors that output modulations of light intensity, based on various microbending configuration, were originally used for this purpose due to their simplicity, ease of operation, and low cost [67]. Recently, due to their high sensitivity for strain measurements, FBGs and long-period fiber gratings (LPFGs) have been used for measurements of respiratory and heart rates, where the miniaturized OFSs were embedded into medical textiles to create wearable inconspicuous sensor devices [68, 69]. These OFSs have been particularly attractive for monitoring the vital signs of patients in MRI scanners due to their EMI and electrical insulation [70]. Besides strain-based monitoring, FBGs were also employed for measurements and analyses of arterial pulse waveforms, which make FBGs good diagnostic tools for clinical examinations and investigations of cardiovascular diseases [71, 72].

In addition to FBG sensors that sense body movements, another approach for monitoring respiration employs optical fiber-based humidity or temperature sensors placed in proximity to the patient's nose or mouth [28, 73–76]. The fundamental basis of this approach is that the exhaled air has higher humidity (~100%) and is warmer than the surrounding air. A miniature micromachined optical breathing sensor based on an agarose-infiltrated PCF was reported, where the humidity variations between inhaled and exhaled breath were measured in real-time for predicting the breathing rate and the breathing status of a patient during respiration [73]. Employing molecular-level self-assembly processing method, a fiber tip FPI interferometer was constructed by multilayered inorganic nanocluster and polymer thin films, showing high sensitivity to variations in humidity [74]. The performance of the prototype sensor was compared with a medical nasal thermistor and showed excellent potential for monitoring advanced breathing airflows. A simple PCF interferometer was demonstrated as a breathing sensor by monitoring humidity [75]. Two collapsed regions at the interfaces between an SMF and a PCF were intentionally fabricated as the cladding mode exciter and combiner by using a modified fusion splicing process. The PCF interferometer was extremely sensitive as the water molecules in exhaled air were adsorbed on or desorbed from the PCF surface.

Optical-fiber-coupled Doppler flowmetry is commonly used for non-invasive blood flow measurements, which relies on the Doppler frequency shift of the input light as a result of light scattering from moving blood cells [77]. The integrated optical fibers play a role in delivering and collecting light to and from the

measurement points. Several optical fiber micromachining processes were also employed in this application, including fusion splicing, high-accuracy cleaving, and laser micromachining. For example, fiber-in-line collimators including a quarter-pitch graded-index fiber and a micro-spherical lens at the tip of the delivery fiber were fabricated to enhance the performance of the Doppler flowmetry system [78].

1.4 Biochemical Sensors

In addition to physical sensors, in recent years, OFSs have been extensively explored for measuring a variety of chemical and biological parameters due to their unparalleled features, such as miniaturization, high sensitivity, and low limits of detection (LoD). Traditional OFSs (e.g., refractometers) are not yet suitable for biochemical applications due to their chemical non-specificity and non-selectivity, indicating that these types of sensors are not capable of detecting a particular measurand of interest in a complex matrix with other interfering measurands. Consequently, two approaches were developed to empower OFSs with selective responses, including fiber EW spectroscopy (FEWS) and functional-film-assisted OFS. FEWS relies on the fact that a wide range of biochemical molecules have vibrational modes in the fingerprint region localized in middle infrared (mid-IR) spectral range, allowing direct analysis of the spectrographs of analytes due to the interactions between the EW and the analytes [79, 80]. The optical fibers used in FEWS are typically made of IR-transparent materials, such as chalcogenide glasses, and fluoride or silver halide glasses, which support low-loss propagation of IR optical signals. FEWS has been used in a variety of applications, such as for the detection of pollutants in wastewater, online monitoring in chemical, industrial, and food processes, and biosensing [81–83]. A concern regarding the potential toxicity of the IR fibers (e.g., chalcogenide glasses) in biological systems was reported [84].

In a functional-film-assisted OFS, a chemically selective and sensitive functional coating is deposited onto the fiber surface of the OFS. The optical properties of the functional coating vary when it interacts with an analyte of interest, and the variations can be transformed into changes in the properties of the light propagating in the OFS. By analyzing the changes in the reflection/transmission spectrum derived from the OFS, quantitative and qualitative information of the chemical analyte can be obtained. The basic idea is the coupling of a highly sensitive OFS probe to a functional coating to form a biochemical sensor device. Separately, neither the OFS nor the functional coating functions as a practical sensor due to the chemical non-specificity of the former and the challenge in signal transduction of the later. However, combining the prominent advantages of the two (i.e., high sensitivity and chemical selectivity, respectively) offers a universal strategy, which applies to various functional coatings and consequently many analytes. Moreover,

the functional-film-assisted OFS motif offers the prospect for the development of compact, portable, and low-cost devices combined with cheap light source (e.g., LED) and photodetector. The operational wavelength of this type of OFS is defined by the coating properties instead of the absorption features of the analytes, which provides great design flexibility.

1.4.1 Biosensors

In optical fiber biosensors, biological recognition molecules are bound to an OFS for the detection and quantification of specific biological analytes. The biological components can convert the recognition event into changes in the optical properties, which can be probed by the OFS. The changes in the optical properties may render in the form of fluorescence (e.g., emission or quenching), changes in absorbance, variations in the index of refraction, chemiluminescence, etc. Typical biological molecules can be enzymes, antibodies, nucleic acids, proteins, or whole cells, and are chosen for their specificity and affinity [85].

In general, optical fiber biosensors are configured for two modes: labeled and label-free detections. Fluorescence-labeled detection was widely employed in biosensors in earlier years, where the sensors utilize fluorescence labeling of the analytes of interest and monitor the variations in the fluorescence intensity induced by the interaction between the analyte and the biological recognition molecules [86, 87]. In recent years, label-free detection has been extensively proposed and demonstrated due to its low cost and ease of operation, where the complex labeling procedures and associated problems in fluorescence-labeled detection are avoided (e.g., short lifetime and photo-bleaching of the dye). Label-free detection typically relies on the measurement of changes in optical thickness, defined as the product of the index of refraction and physical length, induced by the binding of analytes of interest to the biological recognition molecules. In the construction of these sensors, typically, an OFS sensing platform with enhanced EW is preferred, such as a polished fiber and a tapered fiber, where the biological recognition molecules are deposited on the region where the fiber diameter is reduced [88–91], as shown in Fig. 3.

Besides these tapered or polished fiber-based OFS, long-period fiber grating (LPFG)-based optical fiber refractometers have also been demonstrated as a promising platform for label-free biosensing [92–97]. An LPFG is a core-cladding mode coupling device, where the high attenuation of the cladding modes results in a series of resonance bands centered at discrete wavelengths in the transmission spectrum, with each resonance band corresponding to the coupling of a different order of cladding mode [98]. The interaction between the cladding modes and the surroundings in an LPFG can provide precise analytical information about the optical thickness of the coating layer. Figure 4a illustrates the effect of the surrounding refractive index changes on the transmission spectrum

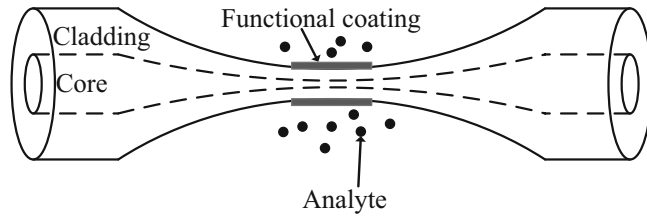


Fig. 3 Schematic illustration of a functional-film-assisted tapered OFS for biochemical sensing

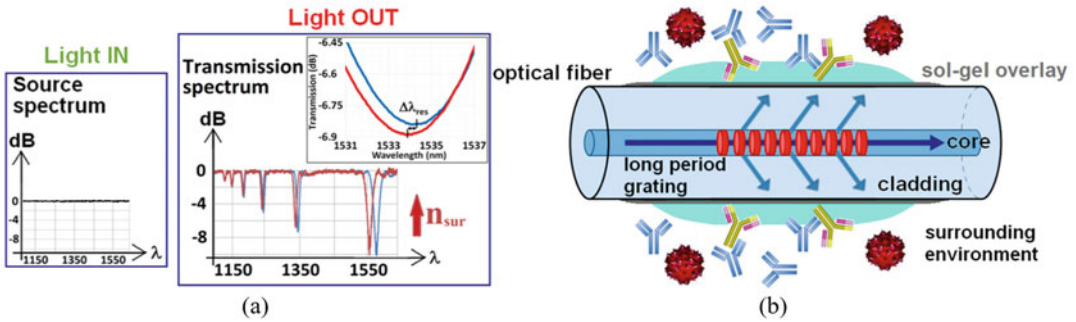


Fig. 4 Schematic illustrations of the response of an LPFG to a change in the refractive index of the surrounding and an LPFG-based biosensor. (a) Schematic illustration of the effect of the surrounding refractive index changes on the transmission spectrum of an LPFG. (b) Schematic of a functional-film-assisted (sol-gel overlay) LPFG for biosensing [96]

of an LPFG. Typically, LPFGs are designed to operate at the phase matching turning point (PMTT) in biosensing, which provides the highest sensitivity to the surroundings. An LPFG coated with a thin film of biotin-modified silica core gold shell ($\text{SiO}_2:\text{Au}$) by a layer-by-layer method was reported for streptavidin detection with the LoD of 2.5 nM [92]. A traditional sol-gel dip-coating technique was also employed for coating functional film onto the surface of an LPFG, where the thickness of the film overlay could be flexibly controlled by adjusting the sol viscosity and the withdrawal speed during the dip-coating process, as shown in Fig. 4b. A sol-gel-based titania-silica-coated LPFG functionalized with a methacrylic acid/methacrylate copolymer integrated immunoglobulin G (IgG) was proposed as an effective and feasible label-free biosensor for the detection of anti-IgG with LoD of 10^{-11} M [96]. LPFG-based biosensors are also widely used for label-free DNA detection and quantification in complex DNA samples [93–95].

Another widely used configuration for label-free biosensing is a plasmonic OFS, which constitutes miniaturized counterparts to a traditional (localized) surface plasmon resonances (SPR) system where bulky prisms and microscopes are used [99]. In the construction of optical fiber SPR biosensors, a thin metal layer (e.g., gold, ~50 nm) or nanoparticles (NPs) are deposited on a

micromachined optical fiber for SPR/LSPR generation where the EW is enhanced and brought in direct contact with surroundings; bioreceptors or biological recognition molecules are then grafted and immobilized on the metal surface through covalent bonding [100]. The EW excited SPR/LSPR is highly sensitive to the binding of analytes to the bioreceptors. The plasmonic OFS is usually spectrally interrogated, where changes in the transmission or reflection spectra are measured. Most of the plasmonic OFSs operate at visible wavelengths (e.g., 500–800 nm). Compared to other optical fiber refractometer-based biosensors, the most advantageous feature of plasmonic OFSs is the high sensitivity and low LoD.

A variety of micromachined optical fibers have been investigated as building blocks for plasmonic OFSs. The most straightforward way of bringing the core-guided light in direct contact with the surroundings is to remove the silica cladding entirely or partially through chemical etching or side-polishing [101–104]. Except for the polished D-shaped fibers, another similar configuration fabricated by femtosecond laser micromachining was also proposed, where a narrow trench in the fiber cladding was ablated [105]. Self-assembled gold colloids were deposited onto the surface of the trench to produce LSPR for refractometry. The refractometric sensitivity of polished fiber-based plasmonic OFSs can reach 4000 nm/RIU (RIU, refractive index unit) [100]. Unclad fibers with cores directly exposed to the surrounding medium were also employed for plasmonic OFSs. An unclad fiber with a silver and silicon coating on the core followed by immobilization of an enzyme (glucose oxidase) using gel entrapment was demonstrated for low concentration glucose measurements [106]. Another building block for developing plasmonic OFSs is the tapered fiber, where the EW in the tapered region is greatly improved. Coating a thin noble metallic layer over the tapered region results in an SPR refractometer [107–111], where the sensitivity reaches up to 11,800 nm/RIU. A dielectric layer (e.g., indium nitride) was also explored as an SPR material [108]. Functionalizing these highly sensitive refractometers with specific bioreceptors makes it possible to develop selective biosensor with a low LoD. Hetero-core structures, realized by simply fusion splicing two types of fibers with different core diameters (e.g., SMF and thin-core fiber), have also been used in plasmonic OFSs [112]. The core mismatch couples core-guided light to cladding modes, which can excite plasmonic interactions at the outer surface of the sensing fiber when it is coated with a metal layer. The hybrid structure could be bent or tapered to further enhance the EW field in the sensing region, thus improving the measurement sensitivity [113, 114]. Bending a fiber is the most straightforward approach for bringing core-guided light to cladding modes due to the perturbations of the total internal reflection (TIR). Assisted by heating using a flame, U-shaped

structures with a bend radius as small as 0.5 mm were successfully obtained with satisfactory repeatability [115, 116]. Gold nanoparticles (GNPs) were bound to the U-bent region to excite LSPR, which was then functionalized with IgG as the bioreceptor for the detection of anti-IgG.

Instead of mechanically or chemically removing the cladding to access the core-guided light, grating-assisted fibers were also explored for the implementation of plasmonic OFSs without degrading the mechanical integrity of the silica optical fibers. LPFG has been demonstrated for this purpose due to the coupling core mode to cladding modes, which can excite a surface plasmon wave (SPW) [117, 118]. A traditional FBG is not suitable for plasmonic sensing since the light is confined in the fiber core, making it insensitive to changes in the surrounding medium. Tapering and chemical etching are effective approaches used to access the core-guided mode in an FBG [119, 120]. In recent years, a tilted FBG (TFBG) has been proposed with grating fringes that are not perpendicular to the axial direction of the fiber core. Cladding modes are consequently excited due to the tilted grating pattern, resulting in a dense comb-like transmitted amplitude spectrum with a series of narrowband cladding mode resonances on the short wavelength side of the Bragg resonance [121]. One attractive feature of a TFBG is that the Bragg resonance is immune to the surrounding medium, indicating that the Bragg resonance can be used to compensate for unwanted interference coming from temperature variations or light source power fluctuations. Assisted with a thin metal layer on the grating region, TFBGs have been demonstrated as plasmonic OFSs [122–125]. Compared with other plasmonic OFSs, the transmission spectrum of a TFBG-based sensor is a fine comb of narrowband resonances that overlap with the broader SPR resonance, providing a unique approach to accurately detect tiny shifts of the plasmonic resonance. A gold layer-coated TFBG, functionalized with a thrombin-binding aptamer was demonstrated to detect the protein human α -thrombin in its fibrinogen-binding exosite, as schematically shown in Fig. 5a [126]. The authors of the work also proposed a multiplexed TFBG-SPR device assisted with a fluidic channel, where multiple sensors could be embedded, as presented in Fig. 5b. Each of the SPR sensors can be functionalized with different bioreceptors to capture different targets, to provide a baseline reference data, or with the same bioreceptors to improve the LoD through statistical analysis of the response of the multiple sensors.

Microstructure optical fibers with air tunnels were also explored for plasmonic generation by coating the holes with NPs or filling some of the holes with metal [127, 128]. Another interesting plasmonic OFS is based on a single-ended optical fiber, where the cleaved end facet of the fiber is patterned or covered

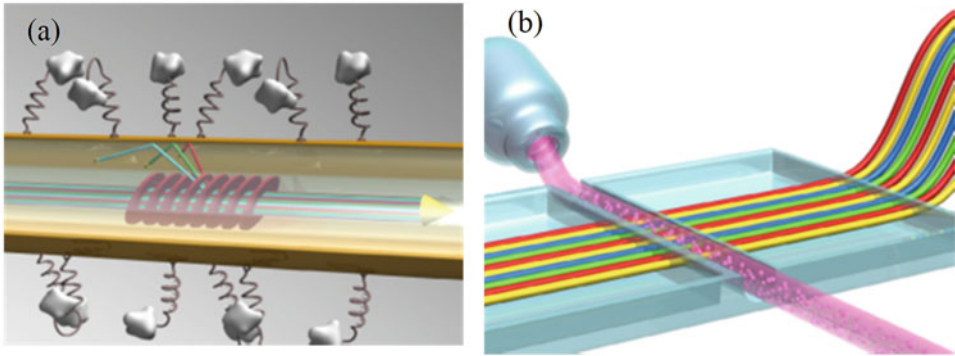


Fig. 5 Schematic of a TFBG-based biosensor and the illustration of the potential multiplexing. (a) Schematic diagram of a gold-coated TFBG-SPR sensor covered with aptamer receptor molecules. (b) Conceptual illustration of multiplexed TFBG-SPR sensors embedded across a microfluidic channel [126]

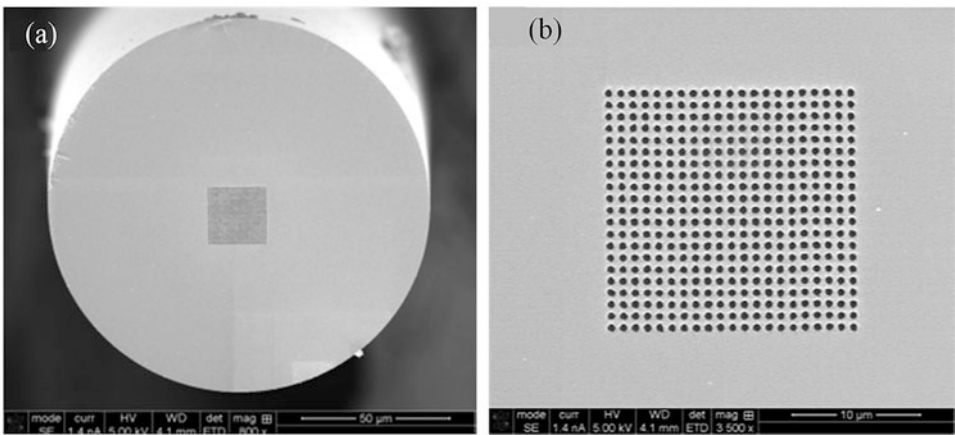


Fig. 6 SEM images of the optical fiber SPR sensor fabricated by FIB micromachining [133]. (a) Overview of the fiber tip endface with the fabricated EOT structure. The diameter of the optical fiber is 125 μm . (b) An enlarged view of the EOT hole arrays on the fiber tip. The size of the holes varied from 522 to 625 nm, and the periods of the hole arrays ranged from 912 to 1056 nm

with an array of NPs [129–133], as illustrated in Fig. 6. In this case, the NPs are directly exposed to the core-guided mode in the fiber, yielding the generation of LSPR. Different approaches were exploited for patterning. For example, E-beam lithography nanofabrication was used to pattern gold nano-dot arrays on the fiber end facet [132]; focused ion beam (FIB) milling machine was used to directly fabricate subwavelength hole arrays on the gold film coated on fiber endface [133]; microsphere photolithography was demonstrated for low-cost fabrication of nano-patterns on the fiber endface [134].

1.4.2 Chemical Sensors

The detection of chemical compounds found in the human body in clinical settings has been extensively explored because it offers the possibility for noninvasive diagnoses of diseases. The detection of compounds could be conducted in the gas phase, where the gas molecules of interest are exhaled in the breath or emitted from the skin; or, in the liquid phase, in liquid samples, such as blood, urine, saliva, and other liquids containing human metabolites.

pH is a significant parameter in biology; it is diagnostic of the functionality of many organs and parts of the human body. Accurate knowledge of pH provides useful and valuable information for the diagnosis of diseases. The pH of fluids in the human body varies over a wide range, depending on the functions of different cells [135]. The most widely used approach of optical fiber-based pH sensors relies on the use of dye indicators, which are immobilized in matrix materials and deposited on a cleaved end facet of an optical fiber [136, 137]. Various pH molecule indicators have been demonstrated for the construction of OFS-based pH devices, including acidochrome dye, fluorescein acrylamide, thymol blue, ethyl violet dye, neutral red, eosin, and other mixtures of organic molecules [138]. These sensors are typically interrogated by measuring changes in the optical properties of the indicator, such as absorbance, fluorescence, and fluorescence lifetime, to determine the variations of pH in the liquid sample. The optical fibers used in these sensors only play a role in delivering excitation light to the pH-sensitive dye and collecting the fluorescence emission. To further miniaturize the sensor head, tapered fibers are employed [139]. One concern for pH-indicator-based OFSs is the long-term deterioration induced by the bleaching of the indicator molecules. In recent years, functional film-assisted OFSs have been exploited for pH measurements, where the optical properties of the film change as a function of pH. Specifically, in OFS-based pH devices, nanostructured films are used, whose morphology, with emphasis on swelling, depends on pH. Since the refractive index (RI) of a swellable film (e.g., polyelectrolyte-deposited nanostructured material) is influenced by pH, one can design pH sensors through the measurement of the external RI. Various micromachined optical fiber refractometers were used as the building blocks for pH sensors, as discussed in the previous section, such as FPI, LPFG, TFBG, hetero-core structures [138, 140–143]. A thin-core fiber modal interferometer deposited with poly(allylamine hydrochloride) and poly(acrylic acid) nanocoating, employing electrostatic self-assembly techniques, was demonstrated as a wide-range pH sensor (2.5–10 pH unit) with a resolution of 0.013 pH unit [138]. The rise and fall times of the sensor were 120 s and 200 s, respectively. A Fabry–Perot nanocavity pH sensor, in which a nanostructured film was prepared on the surface of the fiber end-face, employed white-light interferometry for the measurements of

pH-induced swelling of the film, which in turn was used to determine the pH [140].

Oxygen (O_2) and carbon dioxide (CO_2) are two routinely measured parameters in biomedical applications as they are valuable for the analysis of circulatory and respiratory systems in the human body. Similar to OFS-based pH devices, the most popular approach used by OFS-based O_2/CO_2 sensors also relies on the use of fluorescence indicators attached to the tip of an optical fiber [144]. The optical properties of the indicator molecules change in the presence of O_2 or CO_2 . A single OFS modified with two different indicators (i.e., O_2 and CO_2 -sensitive materials) was demonstrated for the simultaneous measurement of both oxygen and carbon dioxide [145]. These two indicators have the same excitation wavelength but quite different emission maxima, offering the possibility to distinguish the separate responses of the two indicators. In very recent years, metal-organic frameworks (MOFs) were extensively used in the areas of gas separations and storage because their internal physical and chemical properties can be tailored for these applications using the judicious selection of inorganic and organic building blocks [146]. MOFs have also been explored for chemical sensing applications due to the great design flexibility and tailorable chemical selectivity [147]. Optical fiber CO_2 sensors based on an LPFG coated with a thin layer of MOF (HKUST-1) or an etched optical fiber coated with ZIF-8 were proposed for the detection of CO_2 with high sensitivity as shown in Fig. 7 [148, 149]. These MOF-integrated OFSs rely on the refractive index-based sensing mechanism, where the use of a MOF-based sensing layer results in an amplification of the increasing values of the effective refractive index associated with the adsorption of gases.

The identification and quantification of ammonia are also of interest in biomedical applications due to their correlation to specific diseases, such as dysfunction in the kidney and liver [150]. The detection of ammonia in exhaled air or urine provides a valuable clue for the early diagnosis of some diseases, where typically a sensor with an LoD of 50–2000 ppb and quick response time is desired [150]. Although OFSs have not been demonstrated for detecting ammonia in an individual's breath as of yet, due to the limited measurement sensitivity and LoD, the development of OFS-based ammonia sensors continues. Traditional optical fiber ammonia sensors rely on measuring the change in fluorescence intensity of a buffered pH indicator solution, where the presence of ammonia increases the pH of the solution [151]. More recently, functional film-assisted OFSs have been explored for ammonia gas detection [152–157]. Zinc oxide (with graphene oxide) and polyaniline are the most widely used coating materials for ammonia gas sensors, and various optical fiber structures are used as the sensing

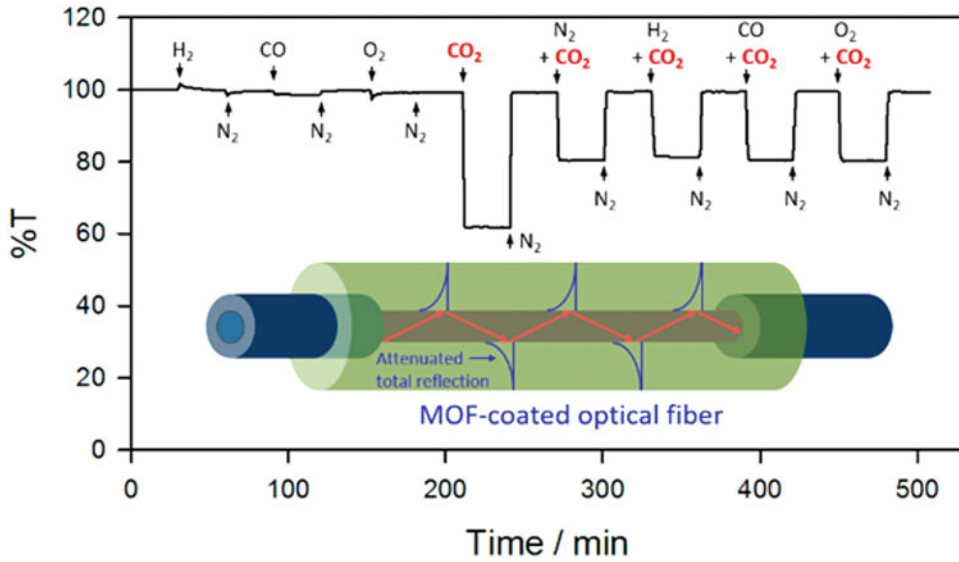


Fig. 7 Etched optical fiber-based CO₂ sensor integrated with a thin film of MOF material. The light transmission of the sensor structure as a function of time is plotted above the sensor element [148]

platform, such as LPFG, tapered fibers (micro/nanofibers), hetero-core structures, FPI.

In addition to sensing ammonia, the detection of volatile organic compounds (VOCs) has attracted great interest due to the high potential as a noninvasive early detection and diagnosis of microbial diseases. The relationship between the VOCs emitted from the human body and a disease or disorder was reported extensively [158]. A variety of “electronic noses” have been developed to detect and discriminate between the production profiles of VOCs from microbial infection in situ [159–162]. Combined with artificial intelligence and web-based knowledge systems, electronic noses were expected to have a valuable role in monitoring disease epidemiology [162]. The use of OFSs for this purpose has also been proposed. Compared to the electronic nose (e.g., an array of chemical sensors), OFS-based sniff systems provide significant advantages, such as small size, lightweight, ease of fabrication, low fabrication cost, and capability of multiplexing employing a single fiber. Preliminary studies have shown that a micromachined EW-based OFS modified with a functional layer (i.e., dye compound) was able to distinguish skin emissions from several different volunteers in the test [163]. Taking advantage of optical fiber micromachining techniques, several OFS-based VOC sensors have been demonstrated recently based on functional film-assisted configurations, i.e., micromachined optical fibers (e.g., LPG, tapered fiber, etc.) deposited with a sensitive layer [164–166]. These sensors do not yet play a meaningful role in medical applications due to insufficient sensitivity and chemical selectivity.

Humidity is another important quantity that is often measured and monitored in clinical settings. Humidity measurements not only can be used for respiratory monitoring (as discussed in the previous section) but also play a significant role in the monitoring of gas mixtures delivered to patients from ventilator care equipment [167]. In these applications, humidity sensors with fast response times and recovery times (e.g., <1 s) are required. One of the most popular configurations of OFS humidity devices is the FPI, where various humidity-sensitive films are employed to construct a micro Fabry–Perot cavity on the tip of an optical fiber [168]. The operational principle of these sensors relies on the detection of the RI change or swelling induced by the absorption of water molecules into the film. In addition to FPI configurations, other humidity-sensitive film-assisted structures, such as TFBG, tapered fibers, U-bend structures, LPFG, etc., have also been demonstrated for humidity sensing [169–171]. Very recently, graphene (oxide) has attracted a great deal of interest as the sensitive film for humidity sensing due to its two-dimensional structure of one-atom thickness, high specific surface area, chemical stability, and optical properties [172, 173], which can potentially provide an ultra-fast response to variations in humidity. A fiber-tip Fabry–Perot humidity sensor modified with a ~ 300 -nm-thick graphene oxide (GO) film was fabricated (*see* Fig. 8) and exhibited a wide sensing range, spanning from $\sim 10\%$ to $\sim 90\%$ RH, and more significantly, an ultrafast response time of 60 ms and a recovery time of 120 ms [174]. A GO-coated TFBG was also shown to exhibit an ultrafast response time of ~ 42 ms. The rapid response time was due to the unimpeded permeation of water molecules through the GO interlayer [175]. Another important application of humidity measurements involves the monitoring of the microenvironments within chronic wounds [176], where accurate humidity detection enables

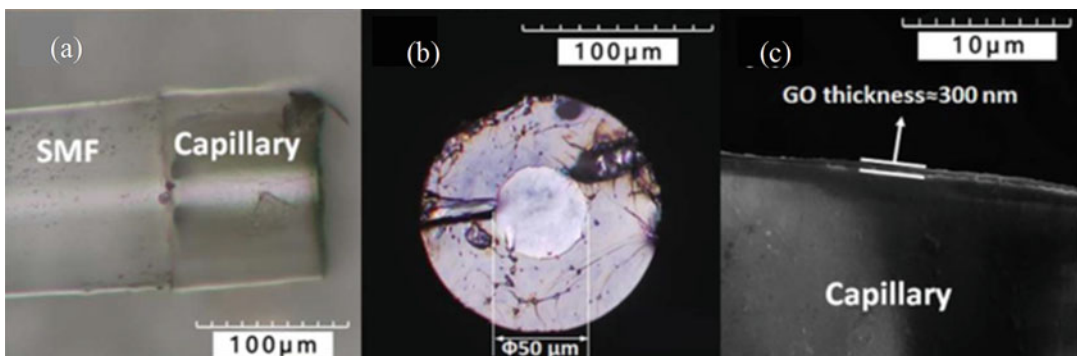


Fig. 8 A fiber-tip FPI-based humidity sensor with a GO diaphragm. (a) Fiber-capillary tip with GO diaphragm. (b) The GO membrane-covered fiber-capillary tip. (c) SEM image of the thickness of the suspended diaphragm [174]

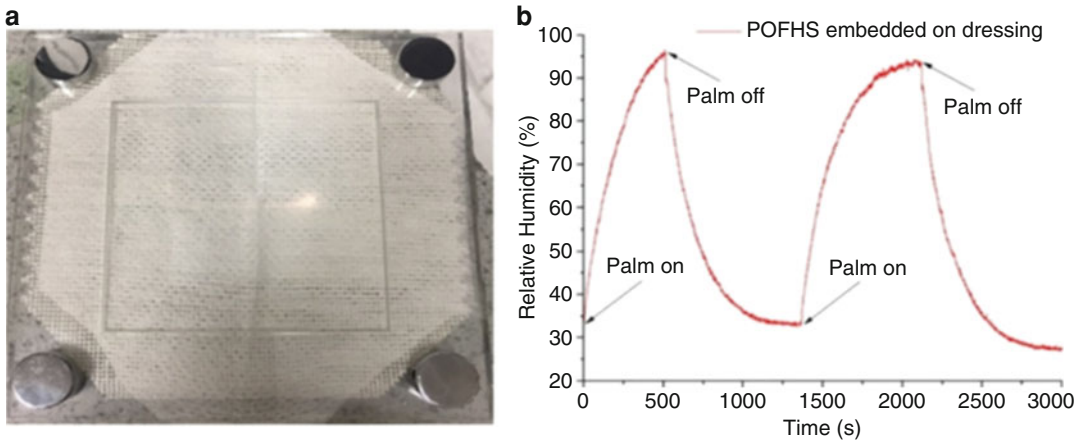


Fig. 9 Proof-of-concept in vivo RH measurement using an OFS humidity sensor. **(a)** OFS humidity device embedded in a wound care dressing and covered by a clinical gauze as a secondary dressing for humidity measurements. The unclad visible part of the sensor is 30 mm long. **(b)** In vivo humidity measurements on the palm of a hand recorded with a humidity sensor embedded in a wound care dressing and covered with a clinical gauze as a secondary dressing [176]. Palm on: placing the hand on the device; palm off: moving the hand away from the device. The settling and recovery times were ~ 7.7 and ~ 9.7 min, respectively. The reason for the long response time was that the sensor was embedded in the dressing and covered by a clinical gauze

appropriate clinical interventions at proper healing stages, thus improving wound care (*see* Fig. 9).

1.4.3 Intracellular Sensors

The capability to monitor microenvironments at the single-cell level has been facilitated by the use of the MNF-based sensing platform, which takes advantage of optical fiber micromachining techniques, especially tapering in this case. The realization of intracellular chemical sensing was first reported in 1992, where a sub-micrometer optical fiber was employed for pH measurements at the single-cell level [177]. The sensor was fabricated by tapering a commercial optical fiber down to a submicrometer size, as small as $0.1 \mu\text{m}$, followed by coating the thin fiber with a layer of aluminum; the endface was left as a transmissive aperture. A copolymer imbued with a pH-sensitive dye was attached covalently to the silanized fiber tip surface using a photopolymerization reaction, as shown in Fig. 10. This micro/nano-machined optical fiber tip sensor simultaneously achieved a thousandfold miniaturization of the probe head, a millionfold reduction of the sample size, and a hundredfold reduction of the response time (< 20 ms) [177]. Since then, optical fiber nanoprobe have been extensively explored for sensing at the molecular and cellular levels in a variety of medical applications [178, 179]. Generally, antibodies, selective for target analyte molecules, are covalently bound to the tip of an MNF. The target molecules bound to the antibody molecules are excited by the strong EW field at the fiber tip when excitation light at a specific wavelength is launched into the fiber. The variations in the

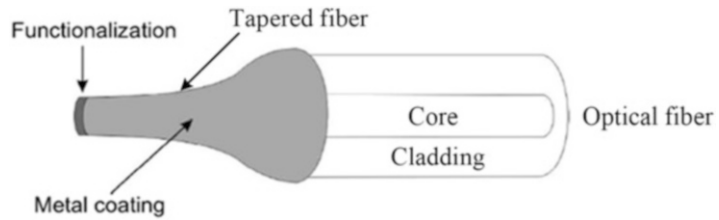


Fig. 10 Schematic illustration of an intracellular sensor based on a functionalized MNF tip [5]

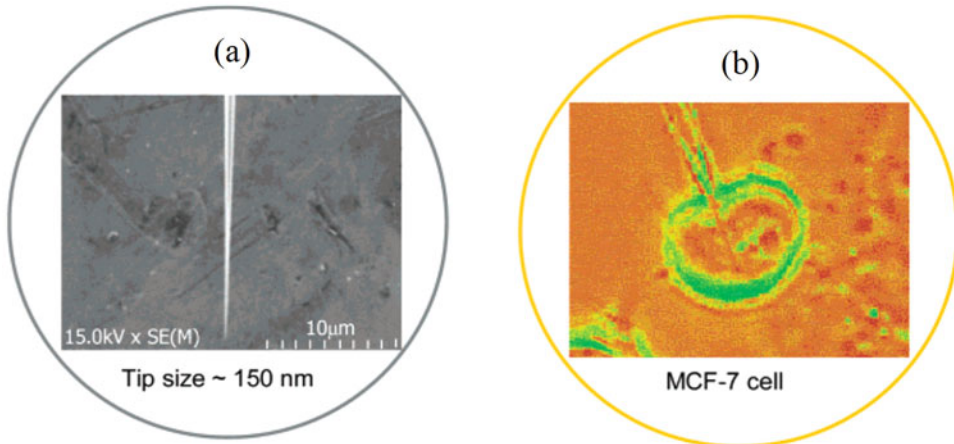


Fig. 11 Nano-machined optical fiber for single-cell applications. (a) SEM image of a nano-tip after coating with 100 nm of silver metal, achieving a final tip diameter of 150 nm. (b) Image of optical nanoprobe inserted into a single live MCF-7 cell [182]

fluorescence emissions from analyte molecules are collected and analyzed to determine the concentrations of the analyte molecules. Antibody-based MNF sensors have been demonstrated for measurements of toxic chemicals contained within single cells (*see* Fig. 11), such as benzo[α]pyrene tetrol, benzo[α]pyrene [180–182]. Many efforts have also been put in improving the excitation and collection of the fluorescence signals by optimizing the geometry of the fiber tip [183, 184]. A hexagonal 1-in-6 fiber configuration enabled by advanced tapering procedures was proposed for intracellular single-cell pH measurements, which enabled the optimal signal collection and minimal interference [183]. In addition to fluorescence-based MNF biosensors, whispering-gallery-mode biosensors excited by tapered fibers were also employed for label-free biosensing down to the level of single molecules [185].

1.5 Lab-in-Fiber

Compact and functional lab-on-chip (LOC) devices on planar or multilayered platforms have kept advancing the biological and chemical laboratory processes [186]. Optofluidic devices, enabled by LOC developments that include combining microfluidic

channels with optical sensing elements, have been exploited to harness the novel opportunities of integrated micro/nanostructure photonics [187]. A migration of integrated LOC devices into optical fiber platforms would open the revolutionary prospect of creating novel lab-on-fiber (LOF) or lab-in-fiber (LIF) devices for multifunctional sensing [188]. Recently, LOF has been extensively investigated for a variety of applications, including label-free chemical and biological sensing, as discussed in the previous sections. One of the main challenges for LOF sensing is bringing the core-guided light to the fiber cladding surface where sensing structures or functional chemicals can be introduced. Several mechanical or chemical strategies have been developed for addressing the challenges of transferring light from the core to the cladding, such as tapering, polishing, chemical etching, femtosecond laser micromachining. These methods are efficient in bringing a strong probing evanescent field to the cladding surface but with the disadvantage of degrading the mechanical integrity and strength of the fibers. On the other hand, the LIF concept provides the revolutionary prospects of optimizing the packaging and densification of multiple sensing elements, which are not possible for LOF. Three-dimensional patterning inside optical fibers by femtosecond laser direct writing, together with selective chemical etching, has been demonstrated as a powerful tool to inscribe all-in-fiber optical waveguides and gratings as well as microchannels and optical resonators [188–191].

An all-in-fiber assembly-free optofluidic device fabricated employing the FLICE technique was reported, consisting of horizontal and vertical microchannels [190]. The horizontal microchannel was conceived as an FP cavity while the vertical one was used as the inlet/outlet to the cavity. The novel device was demonstrated for measurements of the refractive index of the liquids that filled the microchannel. Also, the device afforded unique features, such as great design flexibility, ease of fabrication, mechanical robustness, and miniaturization. A more complicated LIF inside an SMF fabricated by an advanced FLICE technique was demonstrated recently, where optically smooth surfaces (~ 12 nm rms) were realized with ultra-low insertion loss [188]. Cladding waveguides, X-couplers, fiber Bragg gratings, microholes, mirrors, optofluidic resonators, and microfluidic reservoirs were fabricated in an SMF and a spliced piece of coreless fiber. These components were combined and integrated into multicomponent 3D optofluidic fiber sensors with enhanced functionality, improved intelligence, and capability for sensing enriched information (*see* Fig. 12). The LIF system for sensing applications was demonstrated as (1) fluorescence excitation and detection in the microhole through the SMF core waveguide, (2) in-line refractometry through the FPI in a coreless fiber, (3) the combination of a cladding FPI with an FBG for simultaneous measurements of refractive index,

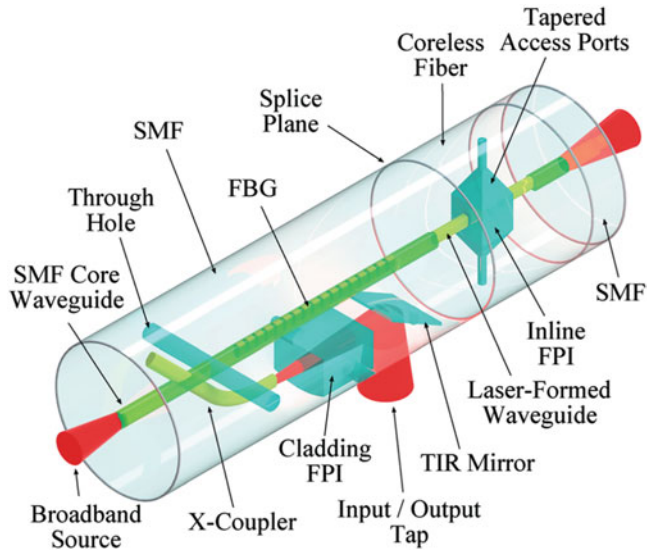


Fig. 12 Schematic illustration of LIF sensing architecture: (1) a through-hole traversing across the SMF core waveguide for fluorescence detection or absorption spectroscopy, (2) an FBG concentric with the SMF core waveguide for temperature or strain detection, (3) an in-line FPI in a coreless optical fiber probed by laser-formed waveguides concentric with the spliced SMF's core for optofluidic applications or pressure sensing, and (4) an X-coupler tap and laser-formed waveguide for probing a cladding FPI for refractive index, pressure, or bend sensing. TIR mirrors are used to tap light either into or out of the fiber cladding for an alternative probing method or for scrubbing undesired cladding modes [188]

temperature, pressure, and bend. The flexible 3D writing techniques and multiplexed sensors were expected to open powerful prospects to migrate the advantages of LOCs into a more flexible and compact platform, optical fibers, via the LIF concept for highly functional and distributed sensing capabilities. Combined with the traditional optical fiber biosensing techniques, a new generation of multiplexed, extremely compact, highly functional, distributed smart biosensors can be developed, e.g., smarter catheter.

2 Materials

A typical OFS system consists of four basic components:

1. Light source, e.g., a tunable laser or broadband laser.
2. Light delivery component, e.g., optical fiber cable, optical fiber coupler, optical fiber circulator.
3. Photodetector or optical spectrum analyzer.
4. Micromachined sensor head.

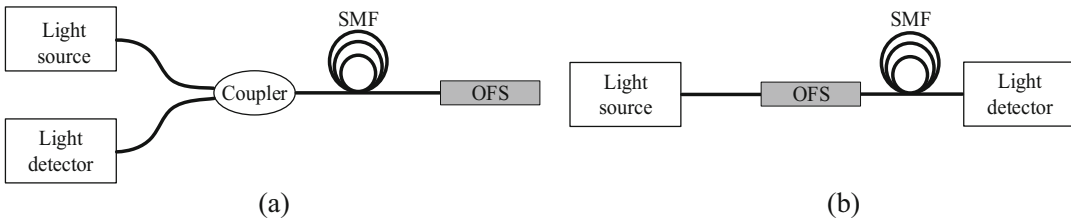


Fig. 13 Typical OFS systems. (a) Reflection OFS system. (b) Transmission OFS system

The light source provides the EM wave for optical interrogation, which is typically a laser, a white light source, or an LED. The light characteristics offer a wide range of properties for different means of interrogation, including intensity, phase, wavelength/frequency, and state of polarization. The light delivery component delivers the light from the source to the OFS and also collects and directs the light from the OFS to the light detector via the same or different optical paths. The delivery component usually includes the optical fiber for light transmission and fiber coupler/circulator for light coupling. The sensor head, i.e., OFS, is essentially the light modulator, which can alter the properties of the input light through the influence of external perturbations (i.e., variations of physical and chemical parameters of interest). In other words, the external perturbations are correlated to the probing light signal via the OFS by modulating the properties of light. The light detector is employed to read and monitor the variations in the properties of the light that is guided back from the sensor head to the interrogator. Different renderings of the changes in the light properties (e.g., intensity variation, wavelength shift, etc.) are used for different OFSs and applications. Figure 13 shows two typical OFS characterization systems: (a) reflection mode and (b) transmission mode. The materials used in four different types of micromachining techniques for fabricating optical fiber sensors are listed below.

2.1 Fusion Splicing

1. Two sections of optical fiber cables that need to be connected.
2. Optical fiber stripper and cleaver.
3. Lint-free Kimwipes.
4. Isopropyl alcohol or acetone.
5. Optical fiber fusion splicer.
6. Optical fiber protection sleeve heat shrinkable tube.

2.2 Tapering

1. A section of optical fiber cable that needs to be tapered.
2. Two motorized linear translation stages.
3. A heat source, e.g., oxy-hydrogen torch.
4. Two optical fiber clamps.
5. Optical fiber stripper.

6. Lint-free Kimwipes.
7. Isopropyl alcohol or acetone.
8. A laser source and a photodetector or an optical spectrum analyzer.
9. Optical microscope.

2.3 Polishing

1. A section of optical fiber cable that needs to be polished.
2. Quartz block with a V-groove.
3. Epoxy.
4. Optical fiber stripper.
5. Optical fiber polishing machine.
6. Polishing powders and polishing pads.
7. Optical microscope.

2.4 Femtosecond Laser Micromachining

1. Femtosecond laser amplifier.
2. A micromachining workstation that includes an imaging system (a camera and a lens assembly), a high-precision three-dimensional translation stage assembly, and lens assembly that directs the laser beam from the laser amplifier to the sample holder on the stage assembly.
3. Two optical fiber magnetic clamps.
4. A section of optical fiber cable that needs to be micromachined.
5. Two sections of spacer fiber.
6. Microscope slide and cover-slip.
7. Index-matching gel.

3 Methods

3.1 Traditional Micromachining

3.1.1 Fusion Splicing

Fusion splicing is the process of joining two optical fibers together by applying high temperature to the interface between the two fibers. The local high-temperature field is usually generated by an electric arc or laser irradiation. Fusion splicing is the most widely used method for connecting two optical fibers either of the same type or different types [192]. Compared to conventional connecting methods such as mechanical connecting, fusion splicing provides the lowest transmission loss and reflectance at the connecting point, as well as offering a reliable and somewhat robust mechanical joint. The instrument used for fusion splicing two fibers is called a fusion splicer. A schematic of a typical optical fiber fusion splicer is shown in Fig. 14b.

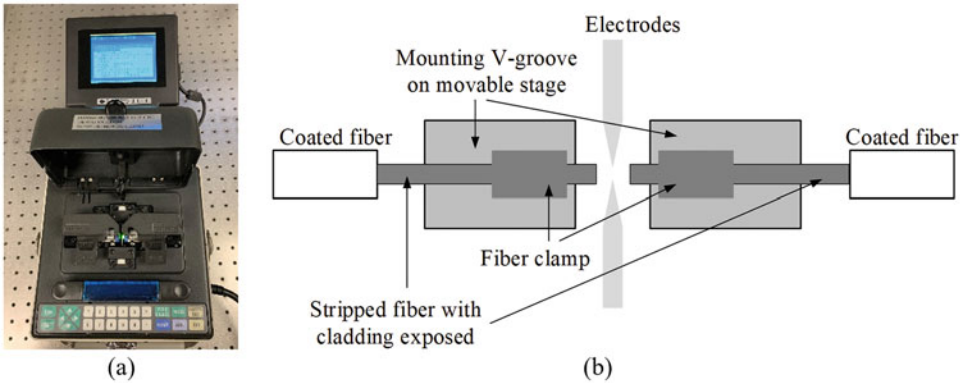


Fig. 14 An overview image and schematic of a typical commercial optical fiber fusion splicer. **(a)** Photograph of a fusion splicer. **(b)** Schematic of a fusion splicer

The process involved in fusion splicing two optical fibers includes stripping, cleaning, cleaving, and splicing. Specifically, the details of the procedures are described as follows:

1. Strip the out jacket, the buffer layer, and the plastic coating to expose a certain length of bare fiber (e.g., 2–3 cm).
2. Clean the fiber to remove residual material and dust using lint-free Kimwipes. Ethanol/acetone is used to moisten the Kimwipe for cleaning fibers.
3. Cleave the exposed bare fiber using a fiber cleaver to get a flat end face.
4. Place the fiber into the fusion splicer and clamp it.
5. Repeat **steps 1–4** above for the second fiber to be spliced.
6. Align the two fibers in the fusion splicer and set the gap between the fiber endfaces to approximately 1 mm.
7. Choose the appropriate fusion splicer program (including the arc power and arc time duration, etc.) and execute the program (*see Note 1*).
8. Remove the fusion-spliced contiguous fiber, and if appropriate, protect the spliced fiber section with a rigid heat shrink tube (*see Note 2*).

For advanced fusion splicers, **steps 6** and **7** can be done automatically. Examples of fusion splicing single-mode fibers (SMF) with several different types of optical fibers are shown in Fig. 15. Figure 15a shows a microscope image of the fusion joint of two SMFs; Fig. 15b shows an optical microscope image of a section of hollow-core fiber (HCF) spliced to two SMFs; Fig. 15c shows a microscope image of the fusion joint of an SMF and a photonic crystal fiber (PCF). It should be noted that when fusion-splicing hollow core fibers (e.g., HCF and PCF), the splicing parameters

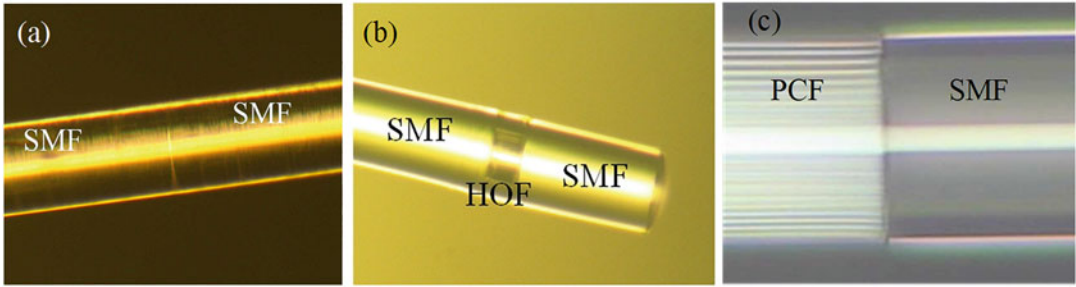


Fig. 15 Examples of fusion splicing single-mode fiber (SMF) with different types of optical fibers. Microscope images of SMF fusion splicing with (a) SMF, (b) hollow-core fiber (HCF), and (c) photonic crystal fiber (PCF) [193]

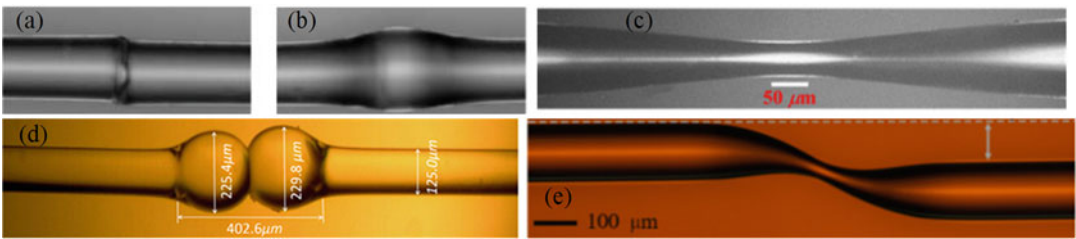


Fig. 16 Examples of advanced fiber in-line structures fabricated by various advanced fusion splicing techniques [194–197]: (a) lateral offset, (b) up-taper, (c) down-taper, (d) peanut-shaped structure, and (e) S-taper. These advanced structures could be used as cladding mode excitors in constructing fiber in-line interferometers for sensing applications with improved compactness and enhanced measurement sensitivity and resolution

should be properly chosen to mitigate the micro-hole collapse effect which could induce extra insertion loss.

In addition to connecting two optical fibers, fiber-in-line special structures have also been fabricated using advanced fusion splicing techniques. Figure 16 shows examples of (a) lateral offset, (b) up-taper, (c) down-taper, (d) peanut-shaped structure, and more complicated structures, such as an (e) S-taper. These structures are widely employed as building blocks (e.g., mode exciter and combiner) for constructing micromachined OFSs with improved performance (e.g., compactness, measurement sensitivity, and resolution).

3.1.2 Tapering

Tapering is a process of stretching an optical fiber at an elevated temperature generated by a heat source such as flame, microheater, or CO₂ laser irradiation. A schematic of a typical home-built optical fiber tapering setup is shown in Fig. 17a. The tapering setup includes two motorized linear translation stages separated by a specified distance (e.g., ~15 cm). Each stage has an optical fiber clamp mounted on the top of the stage, which is used to secure the

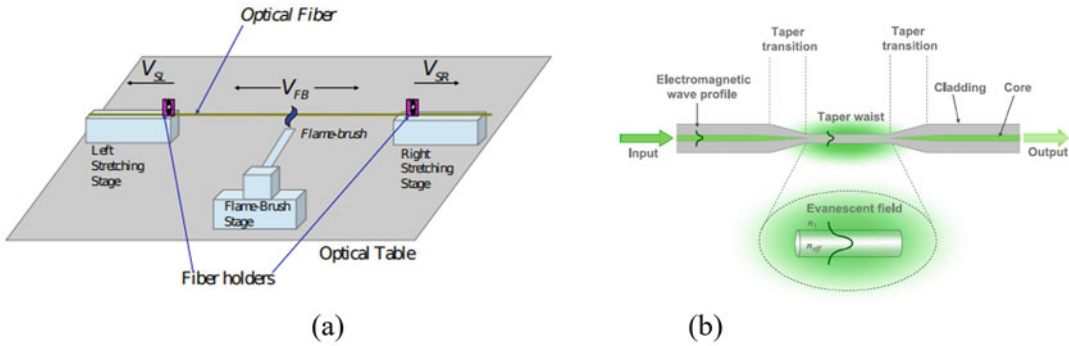


Fig. 17 Schematics of a typical optical fiber tapering setup and a tapered optical fiber. (a) Schematic of a typical home-built setup for tapering optical fibers [198]. (b) Schematic illustration of a tapered optical fiber [43]. A typical tapered optical fiber consists of two regions: the taper waist and the taper transition

optical fiber to be processed. The process involved in tapering an optical fiber is described as follows:

1. Strip the plastic coating in the middle of a section of an optical fiber to expose a certain length of bare fiber (a few centimeters) using the optical fiber stripper.
2. Clean the fiber to remove residual material and dust using lint-free Kimwipes. Ethanol/acetone is typically used to moisten the Kimwipe for cleaning the fiber.
3. Secure the two ends of the optical fiber onto the left and right stretching stages in the tapering setup shown in Fig. 17a with the stripped optical fiber section in the middle between the two stages.
4. Approach the heat source toward the stripped optical fiber section to heat the optical fiber; turn on the motors of the two stages and set them to a constant moving speed.
5. A loss detection system and an imaging system are typically integrated into the tapering setup for monitoring the tapering process in real-time (*see* **Notes 3** and **4**).
6. After reaching the desired parameters of the taper, stop the movements of translation stages and remove the heat source.
7. Remove the tapered optical fiber from the setup and characterize the dimensional parameters of the taper using a microscope.

A tapered optical fiber consists of two regions: the taper waist and the taper transition, as illustrated in Fig. 17b. The tapered waist is a region of fiber with reduced but uniform diameter, while the taper transition is a conical section of fiber where the diameter changes to merge the taper waist with the original lead-in/out fiber. The geometrical parameters of a tapered optical fiber, including the diameter of the taper waist and the transition length, can be precisely controlled by the length of the heating region, heating

time, and the pulling speed of the stages. The processes of tapering optical fibers were initially developed for fabricating directional couplers, where two or more tapers were fused for light coupling. In fact, tapered optical fibers provided several unique features for sensor development, such as compactness, user-configurability, and strong evanescent wave (EW). Generally, the diameter of the taper waist can be reduced down to a few micrometers or even nanometers, making it attractive for biomedical applications where a minimally invasive intrusion is required. More importantly, tapering not only exposes the evanescent field to the surroundings but also increases the evanescent field and penetration depth due to the reduced diameter of the optical fiber, which degrades the confinement of the propagating electromagnetic (EM) wave. The smaller the diameter of the taper waist, the stronger the EW. The enhanced EW will interact with the surrounding medium, making a tapered optical fiber an excellent candidate for chemical/biological sensing. Figure 18 shows several scanning electron microscopy (SEM) images of microfibers/nanofibers (MNFs) fabricated by the tapering technique.

Another application of tapered optical fibers for sensor development is as cladding mode exciter (*see* Fig. 16c), where part of the transmitted light in the optical fiber core is coupled to the cladding when it passes through the tapered region. By employing a pair of in-line tapered optical fibers, a fiber-in-line Mach-Zehnder interferometer can be constructed for sensing applications, such as for measurements of strain and refractive index [202, 203].

3.1.3 Polishing

Fiber polishing is a micromachining technique developed to treat the side cylindrical surface or endface of an optical fiber for proper light guidance. Side-polished fibers are one of the most successful

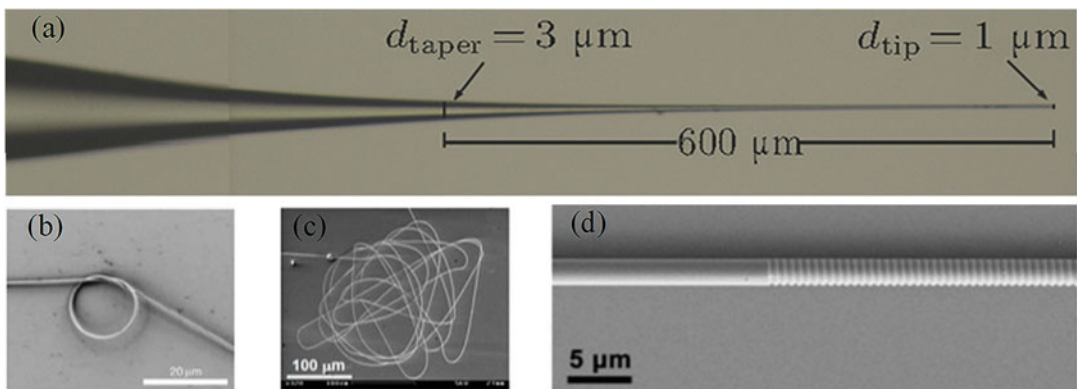


Fig. 18 SEM images of tapered optical fibers with various structural features. (a) A simple tapered fiber tip [199]. (b) A micro-ring made with a 520 nm diameter silica microfiber [200]. (c) A coiled silica microfiber (with a diameter of 260 nm) with a total length of 4 mm [200]. (d) A fiber Bragg grating inscribed on a silica microfiber where the diameter of the fiber was tapered to 1.8 μm [201]

outcomes of the fiber polishing technique. In side-polished fibers, portions of the fiber cladding on one side of the optical fiber are normally removed by the polishing process, as illustrated in Fig. 19a (front view) and b (cross-sectional view), resulting in the exposure of the EW to the surroundings. Side-polished fibers have been extensively studied for evanescent field coupling applications, as well as for sensing due to the enhanced EW in the polished region. Side-polished fibers are also used as a platform for inscribing grating structures for sensing applications [204, 205]. The most significant parameter determining the strength of the EW in side-polished fibers is the thickness of the residual cladding, the thinner the residual cladding, the stronger the EW, thus the stronger the interaction with the external surroundings. Bending the polished region can also greatly enhance the EW, thus improving the sensitivity of the device for sensing applications.

Since optical fibers are generally too small (e.g., with a diameter of 125 μm) to be directly polished alone, blocks used to support fibers during the polishing process are typically required. Quartz or fused silica has been widely used for this purpose because it is essentially the same material as silica fibers. A typical step-by-step side polishing process is schematically illustrated in Fig. 19c and is described below:

1. Strip the plastic coating in the middle of a section of an optical fiber to expose a section of bare fiber with a length that is similar to the length of the V-groove used in the polishing setup (*see Note 5*).
2. Clean the fiber to remove residual material and dust using lint-free Kimwipes. Ethanol/acetone is typically used to moisten the Kimwipe for cleaning the fiber.
3. Place the stripped optical fiber section onto the curved V-groove with the application of a pre-strain.
4. Immobilize the optical fiber in the groove by gluing the fiber (*see Note 6*).
5. Examine the secured optical fiber under an optical microscope to ensure that the central region of the optical fiber sits properly in the groove.
6. Place the block with the embedded optical fiber on the mounting plate that is secured to the polishing jig of a polishing machine.
7. Polish the central region of the optical fiber using polishing powders and polishing pads with appropriate parameters (e.g., grit size $\sim 0.05 \mu\text{m}$, *see Note 7*).
8. Repeatedly clean and wipe the polished surface of the optical fiber during the polishing process.

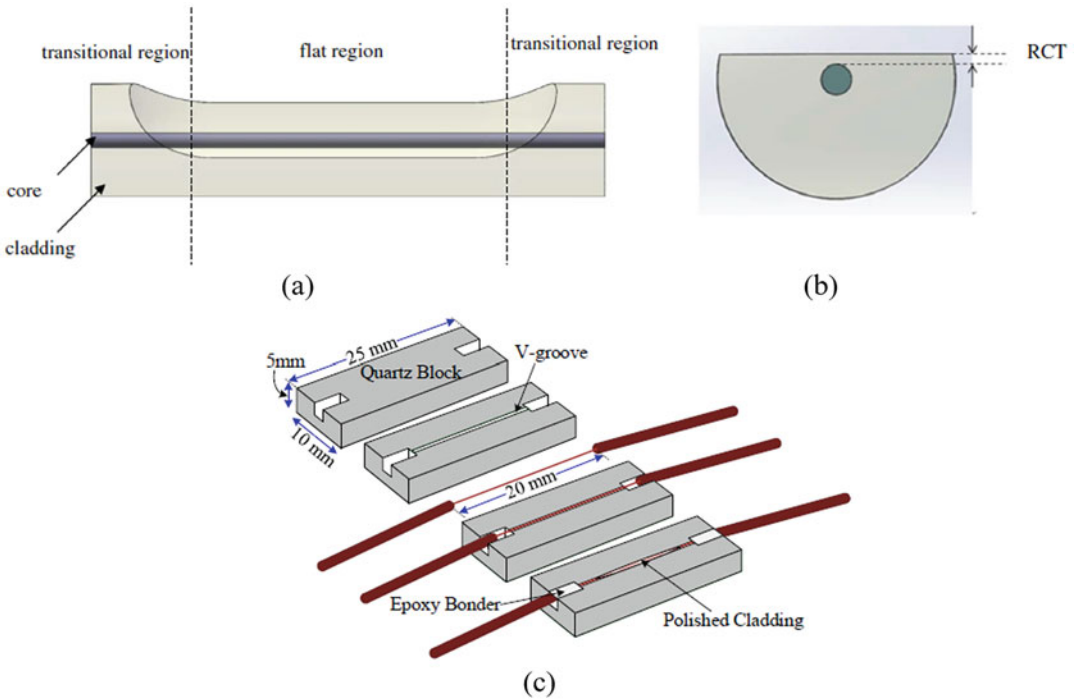


Fig. 19 Overview of a polished optical fiber and the associated fabrication process. Schematic of a side-polished fiber (a) front view and (b) cross-sectional view in the polished region of the fiber. *RCT* residual cladding thickness [206]. (c) Schematic illustration of a typical step-by-step fabrication process for a side-polished fiber [207]

The thickness of the residual cladding after polishing can be estimated by the liquid-drop method [10] or checked under a microscope.

Another application of the fiber polishing technique is endface polishing, where the endface of an optical fiber can be polished to various angles. Optical fibers with angled endface are especially attractive for developing endoscopic probe or imaging device because the direction of propagation of the light output from the optical fibers can be guided to the internal organs and tissues of interest by the angled fiber endface [208]. Figure 20 shows a miniaturized surface-mountable optical fiber pressure sensor with a cross-axial configuration [209]. The cross-axial configuration was enabled by an optical fiber with a 45° angled endface, through which the incident probing light is directed to the sensing diaphragm engineered on the sidewall of the fiber. The cross-axial configuration is especially desirable for pressure measurements in fluids such as in blood vessels because the cross-axial configuration is easy to install and can distinguish the static pressure from the surface flow. The effect of dynamic pressure, i.e., the pressure

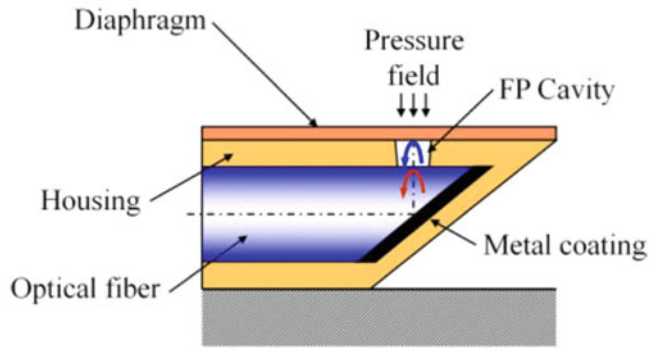


Fig. 20 Schematic of a miniaturized surface-mountable Fabry-Perot (FP) pressure sensor constructed with a 45° angled fiber [209]. The 45° angled fiber was used to direct the incident probing light to the diaphragm engineered on the sidewall of the optical fiber to form the cross-axial configuration

variations induced by the flow hitting at the diaphragm if the diaphragm is perpendicular to the flow, is eliminated.

3.2 Femtosecond Laser Micromachining

Lasers with high intensities have been rapidly developed and used for precise material processing (e.g., welding or cutting) since the first demonstration in the 1960s [210]. With the advancement of laser technologies, especially mode-locking and chirped pulse amplification techniques, the intensities of commercial femtosecond laser (with ultrashort pulse width, in fs scale) have reached up to 10^{13} W/cm². Under the irradiation of lasers with such high intensities, most materials, especially transparent materials, will be ionized and exhibit nonlinear behavior, and consequently undergo a phase or structural modification, leaving behind a localized permanent change in the material (e.g., a change in refractive index or a void space) [11]. In recent years, femtosecond laser three-dimensional (3D) micromachining has found niche applications in material processing and one-step fabrication of photonic micro/nanostructures [211]. Due to the ultra-high intensities, femtosecond lasers can be employed to eliminate materials from the surface of solid structures (ablation) or to transform the local properties within hard or soft solid material structures (irradiation). Compared with traditional long-pulse lasers, femtosecond lasers offer unparalleled features when utilized in fabrication processes, such as high precision, negligible cracks, reduced or eliminated heat-affected zones, and the ability for subsurface 3D fabrication. Femtosecond laser micromachining involves methodologies centered around the interactions and 3D manipulations of femtosecond lasers with materials. OFSs involves methodologies centered around probing-light-measurand encoding and interrogation of the modulated light waves. Combining femtosecond laser

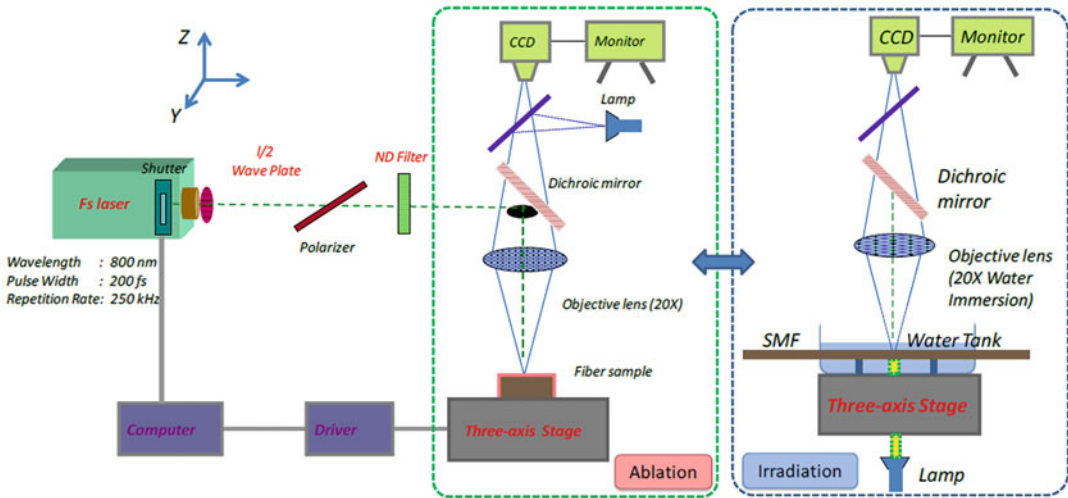


Fig. 21 Schematic of a home-built femtosecond laser micromachining system [189]

micromachining methodologies with optical fiber sensing technologies prompts a new research topic, the lab-in/on-fiber (3D structuring of multiplexed components in/on fiber), which enables the opportunity to fabricate a novel generation of assembly-free smart sensors with combined advantages from the two different arenas.

A home-built femtosecond laser micromachining system is schematically illustrated in Fig. 21. A typical process involved in femtosecond laser micromachining an optical fiber is described below:

1. Load an optical fiber to be processed (with/without polymer coating) in the sample holder on top of a microscope slide. The sample holder is fixed on top of a high-precision translation stage assembly.
2. Secure the optical fiber using two magnetic clamps that are integrated into the stage assembly. A pre-strain is applied to the optical fiber between the two clamps to ensure the fiber section is straight (*see Note 8*).
3. Add two spacers (a small section of an optical fiber) on each side of the secured optical fiber on the microscope slide. Position the two spacers parallel and close to the optical fiber to be processed.
4. Add a drop of index-matching gel on top of the optical fiber to be processed and make sure that the index-matching gel is contained between the two spacers.
5. Place a microscope cover-slip on top of the optical fiber to be processed and make sure that the optical fiber is covered with a

uniform layer of the index-matching gel with no air bubble mixed in the gel.

6. Adjust the focus point of the femtosecond laser beam on the surface of the optical fiber for ablation or within the optical fiber for irradiation, according to the desired purpose, by moving the stage assembly. An online monitoring system composed of a camera and lens assembly is used to assist the alignment and visualize the fabrication process.
7. Open the shutter of the femtosecond laser amplifier for a short period of time (e.g., 20 ms) to cause minute visible damage in the optical fiber to precisely locate the focus point of the laser. Corresponding adjustments of the fiber position can then be made.
8. After fabrication, remove the processed optical fiber from the sample holder for characterization or follow-up chemical treatment.

It should be noted that for the irradiation process, the fiber sample is typically immersed in water, oil, or index-matching gel to eliminate spherical aberrations due to the cylindrically shaped fiber. The properties of the micromachined features on/in an optical fiber are determined by the scanning speed of the translation stage, and the parameters of the femtosecond laser, which include pulse energy, repetition rate, polarization state, and beam profile (*see Note 9*).

3.2.1 Direct Femtosecond Laser Writing in Optical Fibers

Since the discovery by Davis et al. that tightly focused femtosecond laser beams can induce permanent modification to the local refractive index parameter inside a glass, numerous photonic micro/nanostructures have been developed for functional 3D optical circuits in a glass substrate [212]. The unique advantages of 3D femtosecond laser direct writing have also made it attractive to the fiber optic field. Successful examples that have been achieved using femtosecond laser direct writing in optical fibers include grating structures (i.e., fiber Bragg gratings and long-period gratings), ultra-weak in-line reflectors, micro-cavities, waveguides, 3D circuits, and other complex structures (e.g., a micro-cantilever), as shown in Fig. 22. All these microstructures have been demonstrated as building blocks for a new generation of assembly free smart OFS, which are desirable in biomedical applications over traditional OFSs due to the extreme compactness, robustness, improved flexibility, and enhanced functionality and intelligence.

In femtosecond laser direct writing of optical fibers, the accuracy of fabricating design elements of 3D microstructures strongly relies on the size of the focused laser spot. The relationship between the radius of the laser spot (r) and the numerical aperture (NA) of the objective lens used in the femtosecond laser system is approximated by [215]:

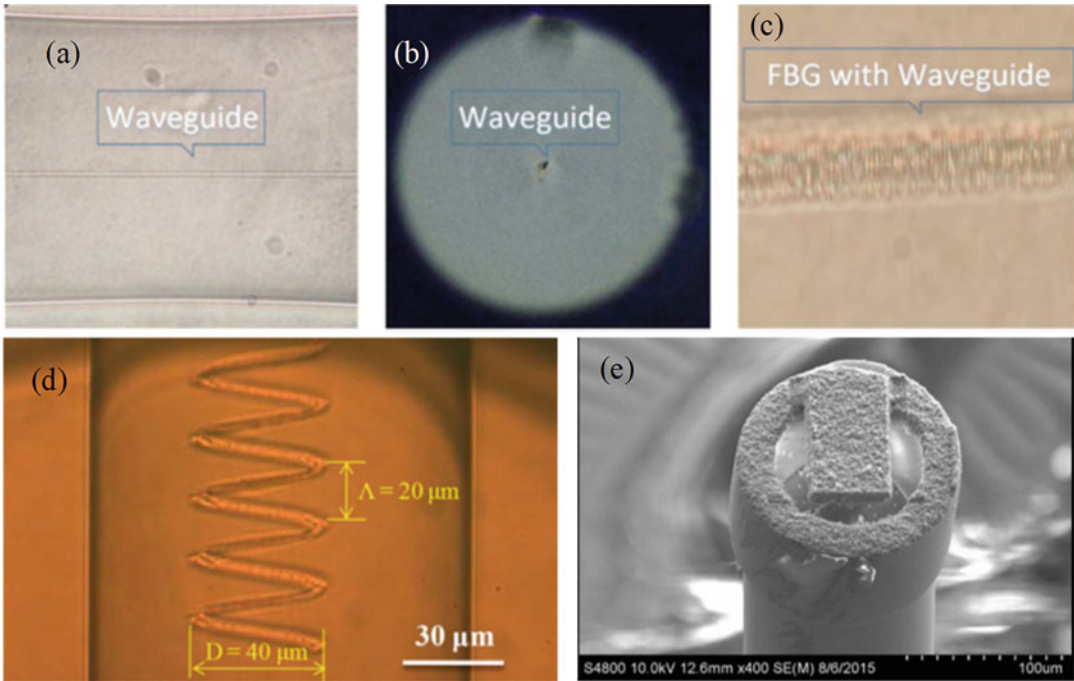


Fig. 22 Examples of microstructures created on/in optical fibers by direct femtosecond laser writing. Microscope images of a waveguide-integrated fiber Bragg grating (FBG) device: (a) waveguide written in coreless fiber, (b) cross-sectional view of the device, and (c) FBG written in the waveguide [213]. (d) Microscope image of a helical structure in an optical fiber [189]. (e) SEM image of a micro-cantilever on the tip of an optical fiber fabricated by femtosecond laser ablation [214]

$$r = \frac{0.61}{NA} \frac{\lambda}{n} \quad (1)$$

where λ is the wavelength of the femtosecond laser beam, and n is the refractive index of the fiber sample. For a given femtosecond laser micromachining system (fixed λ) and a given fiber sample, the larger NA will contribute to a smaller laser spot, resulting in greater accuracy of fabrication. However, there is always a tradeoff between fabrication time and accuracy. A general guide to choosing a proper objective in a femtosecond laser direct writing system is given by the following three guide points [189]:

1. Choose a microscope objective with a low NA (<0.1) for the rough fabrication of large-area surface elements.
2. Choose a microscope objective with an NA ranging from 0.1 to 0.5 for subsurface modification and high-precision surface ablation.
3. Choose a microscope objective with a large NA (e.g., liquid immersive lens) for high-accuracy modifications and ablation of a fiber.

3.2.2 Chemical-Assisted Femtosecond Laser Writing in Optical Fibers

In recent years, optofluidic systems have attracted extensive research interest due to their unparalleled features for chemical, biological, and biomedical sensing applications [187]. In an optofluidic-based system, microfluidic architectures are synergistically integrated into an optical waveguide, where the liquid of interest with an extremely small volume (e.g., microliter, nanoliter, or picoliter) can travel through the microfluidic architectures (e.g., microchannels) and then be analyzed using optical methods. Femtosecond laser irradiation followed by chemical etching (FLICE) has recently emerged as a promising method for fabricating microfluidic systems in waveguides [216]. The combination of the FLICE technique with femtosecond laser 3D direct writing in optical fibers has afforded a novel means of integrating optical circuits and microfluidic systems, which enables the emergence of ultra-compact, alignment-free all-in-fiber optofluidic devices [190]. Specifically, the FLICE technique relies on the high susceptibility of the femtosecond laser-irradiated region to chemical etching, such as hydrofluoric acid (HF) and potassium hydroxide (KOH). Employing the femtosecond laser direct writing technique, arbitrary 3D optical circuits can be fabricated inside an optical fiber. After laser irradiation, the etching process can be conducted. The etching rate of the laser-irradiated region is up to two orders of magnitude faster than that of the un-irradiated region in the fiber cladding. Given sufficient etching time, satisfactory quality of microfluidic architectures with good surface roughness can be obtained. Compared to holey fiber (e.g., PCF)-based optofluidic devices, a FLICE-enabled lab-in-fiber offers much higher flexibility, where multi-microfluidic components can be integrated in 3D to achieve highly functional and multiplexed optofluidic sensing. Figure 23 shows several examples of microchannels fabricated in optical fibers using the FLICE technique.

In addition to FLICE-enabled fabrication of 3D microfluidic systems, an arbitrary microchannel can also be directly fabricated in an optical fiber using the femtosecond laser-induced water breakdown (FLIWD) method, where no hazardous chemicals are required [218]. The FLIWD technique relies on the interaction between the femtosecond laser and the water breakdown phenomenon. Compared to the FLICE technique, the FLIWD approach provides a more uniform diameter of the microchannel. However, in FLIWD micromachining, the surface roughness degrades and thus introducing significant insertion loss [189].

4 Notes

1. The model of the fusion splicer used in the fabrication was TYPE-36, Sumitomo Electric Industries, Ltd. The parameters for splicing two single-mode fibers were as follows: an arc

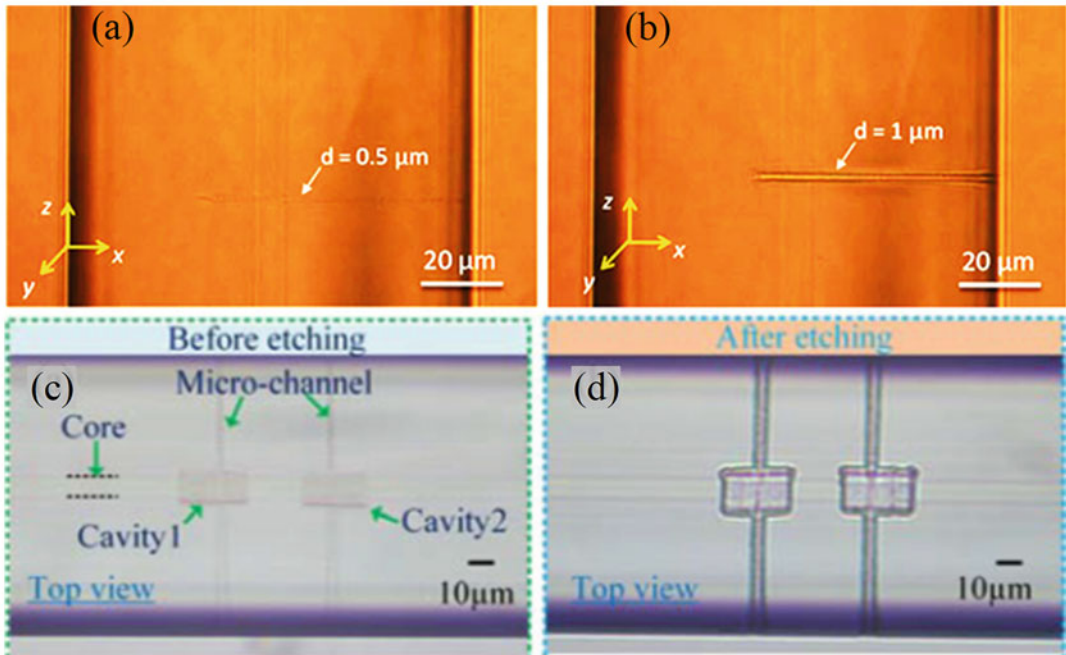


Fig. 23 Examples of microfluidic architectures in optical fibers fabricated by the FLICE method. Microscope images of a blind microhole inside an SMF (a) before HF etching and (b) after HF etching [189]. Microscope images of an all-in-fiber optofluidic device (c) before HF etching and (d) after HF etching [217]

duration of 1.5 s, a prefusion of 0.1 s, an arc gap of 10 μm , an overlap of 15 μm , and an arc power of 64 steps. Note that for splicing a single-mode fiber with a hollow-core fiber, the arc duration and arc power should be correspondingly decreased to avoid the collapse of the hollow-core fiber at the joint point.

2. The fusion-spliced joint is not as strong as the original optical fiber, so a protective sleeve (e.g., a heat-shrinkable tube) is usually used to cover the joint and to protect it.
3. A loss detection system is always integrated with an optical fiber tapering setup for in situ monitoring of the transmission loss of the fiber under tapering. Two free ends of the optical fiber to be processed are connected to a laser source and a photodetector (or an optical spectrum analyzer).
4. A complete optical fiber tapering setup is also integrated with an imaging system (e.g., a microscope or simply an objective combined with a camera) for visualizing the tapering process such that the process can be immediately ceased once the desired dimensional parameters of the optical fiber taper are reached.
5. The parameters of the side-polished fiber, i.e., the length of the polished region and the thickness of the residual cladding, are

determined by the geometric parameters of the V-groove in the supporting block (the length, width, and depth of the groove).

6. In the immobilization of the optical fiber in the polishing process, epoxy should be applied to the central region of the optical fiber in the groove, and the fiber sections in the outer region should be glued after the applied epoxy in the central region cures. The process is necessary to minimize the possible motion of the optical fibers in the central region that will be polished.
7. Cautions should be taken in selecting an appropriate particle size of the powder and the proper polishing pad. If the particle size is too large ($>1 \mu\text{m}$), a large number of scratches could be created on the polished fiber surface, which randomly scatter transmission light.
8. It is necessary to apply a pre-strain to make the fiber straight when the optical fiber to be processed is secured using the two clamps. This process will greatly facilitate the subsequent alignment process especially when a relatively large structure (in length) needs to be fabricated, e.g., a fiber Bragg grating with a length of 5 mm.
9. The properties of the fabricated structure by femtosecond laser irradiation depend not only on the parameters of the femtosecond laser (including pulse energy, repetition rate, polarization state, and beam profile) but also on the movement of the translation stage during fabrication, coupled with the alignment accuracy. An example includes using the femtosecond laser to write a fiber Bragg grating structure by the point-by-point technique. During the fabrication, the translation stage moves at a constant velocity (v) along the longitudinal axis of the fiber; femtosecond laser pulses with a constant repetition rate are focused into the fiber core to cause a localized change in the refractive index. Each laser pulse produces a single grating line in the fiber core. The Bragg wavelength of the fabricated fiber Bragg grating is proportional to the ratio of the velocity of the translation stage to the repetition rate of the laser pulses. Therefore, the point-by-point femtosecond laser inscription of a fiber Bragg grating offers unparalleled design flexibility, where the Bragg wavelength and the index modulation profile can be easily adjusted.

References

1. Bass M, Van Stryland EW (2002) Fiber optics handbook: fiber, devices, and systems for optical communications. McGraw-Hill, New York. vol Sirsi. i9780071386234. Optical Society of America
2. Yeh C (2013) Handbook of fiber optics: theory and applications. Academic
3. Krohn DA, MacDougall T, Mendez A (2014) Fiber optic sensors: fundamentals and applications. Spie Press, Bellingham, WA

4. Edmonson JM (1991) History of the instruments for gastrointestinal endoscopy. *Gastrointest Endosc* 37:S27–S56
5. Meglinski I (2015) *Biophotonics for medical applications*. Elsevier
6. Taffoni F, Formica D, Saccomandi P, Pino G, Schena E (2013) Optical fiber-based MR-compatible sensors for medical applications: an overview. *Sensors* 13 (10):14105–14120
7. Engin M, Demirel A, Engin EZ, Fedakar M (2005) Recent developments and trends in biomedical sensors. *Measurement* 37 (2):173–188
8. Yablon AD (2005) *Optical fiber fusion splicing*, vol 103. Springer Science & Business Media
9. Lou J, Wang Y, Tong L (2014) Microfiber optical sensors: a review. *Sensors* 14 (4):5823–5844
10. Tseng S-M, Chen C-L (1992) Side-polished fibers. *Appl Opt* 31(18):3438–3447
11. Gattass RR, Mazur E (2008) Femtosecond laser micromachining in transparent materials. *Nat Photonics* 2(4):219
12. Schena E, Tosi D, Saccomandi P, Lewis E, Kim T (2016) Fiber optic sensors for temperature monitoring during thermal treatments: an overview. *Sensors* 16(7):1144
13. Lee BH, Kim YH, Park KS, Eom JB, Kim MJ, Rho BS, Choi HY (2012) Interferometric fiber optic sensors. *Sensors* 12(3):2467–2486
14. Choi HY, Park KS, Park SJ, Paek U-C, Lee BH, Choi ES (2008) Miniature fiber-optic high temperature sensor based on a hybrid structured Fabry–Perot interferometer. *Opt Lett* 33(21):2455–2457
15. Tripathi SM, Kumar A, Varshney RK, Kumar YBP, Marin E, Meunier J-P (2009) Strain and temperature sensing characteristics of single-mode-multimode-single-mode structures. *J Lightwave Technol* 27(13):2348–2356
16. Chen P, Shu X (2018) Refractive-index-modified-dot Fabry–Perot fiber probe fabricated by femtosecond laser for high-temperature sensing. *Opt Express* 26(5):5292–5299
17. Zhu C, Zhuang Y, Zhang B, Muhammad R, Wang PP, Huang J (2018) A miniaturized optical fiber tip high-temperature sensor based on concave-shaped Fabry–Perot cavity. *IEEE Photon Technol Lett* 31(1):35–38
18. Jiang L, Yang J, Wang S, Li B, Wang M (2011) Fiber Mach–Zehnder interferometer based on microcavities for high-temperature sensing with high sensitivity. *Opt Lett* 36 (19):3753–3755
19. Hu T, Wang Y, Liao C, Wang D (2012) Miniaturized fiber in-line Mach–Zehnder interferometer based on inner air cavity for high-temperature sensing. *Opt Lett* 37 (24):5082–5084
20. Lu P, Chen Q (2011) Femtosecond laser microfabricated fiber Mach–Zehnder interferometer for sensing applications. *Opt Lett* 36 (2):268–270
21. Zhao Y, Zhao H, R-q L, Zhao J (2019) Review of optical fiber Mach–Zehnder interferometers with micro-cavity fabricated by femtosecond laser and sensing applications. *Opt Lasers Eng* 117:7–20
22. Mihailov SJ (2012) Fiber Bragg grating sensors for harsh environments. *Sensors* 12 (2):1898–1918
23. Chen J, Liu B, Zhang H (2011) Review of fiber Bragg grating sensor technology. *Frontiers of Optoelectronics in China* 4 (2):204–212
24. Mao Y, Zhang Y, Xue R, Liu Y, Cao K, Qu S (2018) Compact optical fiber temperature sensor with high sensitivity based on liquid-filled silica capillary tube. *Appl Opt* 57 (5):1061–1066
25. Yu Y, Li X, Hong X, Deng Y, Song K, Geng Y, Wei H, Tong W (2010) Some features of the photonic crystal fiber temperature sensor with liquid ethanol filling. *Opt Express* 18 (15):15383–15388
26. Geng Y, Li X, Tan X, Deng Y, Hong X (2013) Compact and ultrasensitive temperature sensor with a fully liquid-filled photonic crystal fiber Mach–Zehnder interferometer. *IEEE Sensors J* 14(1):167–170
27. Kuhlmeier BT, Eggleton BJ, Wu DK (2009) Fluid-filled solid-core photonic bandgap fibers. *J Lightwave Technol* 27 (11):1617–1630
28. Yoo W-J, Jang K-W, Seo J-K, Heo J-Y, Moon J-S, Park J-Y, Lee B-S (2010) Development of respiration sensors using plastic optical fiber for respiratory monitoring inside MRI system. *J Opt Soc Korea* 14(3):235–239
29. Jasim AA, Harun SW, Arof H, Ahmad H (2012) Inline microfiber Mach–Zehnder interferometer for high temperature sensing. *IEEE Sensors J* 13(2):626–628
30. J-l K, Feng J, Ye L, Xu F, Lu Y-q (2010) Miniaturized fiber taper reflective interferometer for high temperature measurement. *Opt Express* 18(13):14245–14250
31. Kou J-L, Ding M, Feng J, Lu Y-Q, Xu F, Brambilla G (2012) Microfiber-based Bragg

- gratings for sensing applications: a review. *Sensors* 12(7):8861–8876
32. Xue Y, Yu Y-S, Yang R, Wang C, Chen C, Guo J-C, Zhang X-Y, Zhu C-C, Sun H-B (2013) Ultrasensitive temperature sensor based on an isopropanol-sealed optical microfiber taper. *Opt Lett* 38(8):1209–1211
 33. Hernández-Romano I, Monzón-Hernández D, Moreno-Hernández C, Moreno-Hernandez D, Villatoro J (2015) Highly sensitive temperature sensor based on a polymer-coated microfiber interferometer. *IEEE Photon Technol Lett* 27(24):2591–2594
 34. Talaverano L, Abad S, Jarabo S, Lopez-Amo M (2001) Multiwavelength fiber laser sources with Bragg-grating sensor multiplexing capability. *J Lightwave Technol* 19(4):553–558
 35. Gifford DK, Soller BJ, Wolfe MS, Froggatt ME (2005) Distributed fiber-optic temperature sensing using Rayleigh backscatter. In: 2005 31st European conference on optical communication, ECOC 2005. IET, pp 511–512
 36. Kurashima T, Horiguchi T, Tateda M (1990) Distributed-temperature sensing using stimulated Brillouin scattering in optical silica fibers. *Opt Lett* 15(18):1038–1040
 37. Dakin J, Pratt D, Bibby G, Ross J (1985) Distributed optical fibre Raman temperature sensor using a semiconductor light source and detector. *Electron Lett* 21(13):569–570
 38. Chen Z, Yuan L, Hefferman G, Wei T (2015) Ultraweak intrinsic Fabry–Perot cavity array for distributed sensing. *Opt Lett* 40(3):320–323
 39. Huang J, Lan X, Luo M, Xiao H (2014) Spatially continuous distributed fiber optic sensing using optical carrier based microwave interferometry. *Opt Express* 22(15):18757–18769
 40. Macchi EG, Tosi D, Braschi G, Gallati M, Cigada A, Lewis E (2014) Optical fiber sensors-based temperature distribution measurement in ex vivo radiofrequency ablation with submillimeter resolution. *J Biomed Opt* 19(11):117004
 41. Poeggel S, Durairababu D, Kalli K, Leen G, Dooly G, Lewis E, Kelly J, Munroe M (2015) Recent improvement of medical optical fibre pressure and temperature sensors. *Biosensors* 5(3):432–449
 42. Ukil A, Braendle H, Krippner P (2011) Distributed temperature sensing: review of technology and applications. *IEEE Sensors J* 12(5):885–892
 43. Correia R, James S, Lee S, Morgan S, Korposh S (2018) Biomedical application of optical fibre sensors. *J Opt* 20(7):073003
 44. Roriz P, Ramos A, Santos JL, Simões JA (2012) Fiber optic intensity-modulated sensors: a review in biomechanics. *Photonic Sensors* 2(4):315–330
 45. Cottler PS, Karpen WR, Morrow DA, Kaufman KR (2009) Performance characteristics of a new generation pressure microsensors for physiologic applications. *Ann Biomed Eng* 37(8):1638–1645
 46. Bae H, Yu M (2012) Miniature Fabry-Perot pressure sensor created by using UV-molding process with an optical fiber based mold. *Opt Express* 20(13):14573–14583
 47. Ma J, Jin W, Ho HL, Dai JY (2012) High-sensitivity fiber-tip pressure sensor with graphene diaphragm. *Opt Lett* 37(13):2493–2495
 48. Xu F, Ren D, Shi X, Li C, Lu W, Lu L, Lu L, Yu B (2012) High-sensitivity Fabry–Perot interferometric pressure sensor based on a nanothick silver diaphragm. *Opt Lett* 37(2):133–135
 49. Zhu Y, Wang A (2005) Miniature fiber-optic pressure sensor. *IEEE Photon Technol Lett* 17(2):447–449
 50. Zhu Y, Cooper KL, Pickrell GR, Wang A (2006) High-temperature fiber-tip pressure sensor. *J Lightwave Technol* 24(2):861–869
 51. Guo X, Zhou J, Du C, Wang X (2019) Highly sensitive miniature all-silica fiber tip Fabry-Perot pressure sensor. *IEEE Photon Technol Lett* 31(9):689–692
 52. Donlagic D, Cibula E (2005) All-fiber high-sensitivity pressure sensor with SiO₂ diaphragm. *Opt Lett* 30(16):2071–2073
 53. Cibula E, Pevec S, Lenardič B, Pinet E, Donlagic D (2009) Miniature all-glass robust pressure sensor. *Opt Express* 17(7):5098–5106
 54. Zhang Y, Yuan L, Lan X, Kaur A, Huang J, Xiao H (2013) High-temperature fiber-optic Fabry–Perot interferometric pressure sensor fabricated by femtosecond laser. *Opt Lett* 38(22):4609–4612
 55. Ma J, Ju J, Jin L, Jin W (2011) A compact fiber-tip micro-cavity sensor for high-pressure measurement. *IEEE Photon Technol Lett* 23(21):1561–1563
 56. Liao C, Liu S, Xu L, Wang C, Wang Y, Li Z, Wang Q, Wang D (2014) Sub-micron silica diaphragm-based fiber-tip Fabry–Perot interferometer for pressure measurement. *Opt Lett* 39(10):2827–2830

57. Liu S, Wang Y, Liao C, Wang Y, He J, Fu C, Yang K, Bai Z, Zhang F (2017) Nano silica diaphragm in-fiber cavity for gas pressure measurement. *Sci Rep* 7(1):787
58. Al-Fakih E, Osman A, Azuan N, Mahamud Adikan FR (2012) The use of fiber Bragg grating sensors in biomechanics and rehabilitation applications: the state-of-the-art and ongoing research topics. *Sensors* 12(10):12890–12926
59. Puangmali P, Althoefer K, Seneviratne LD, Murphy D, Dasgupta P (2008) State-of-the-art in force and tactile sensing for minimally invasive surgery. *IEEE Sensors J* 8(4):371–381
60. Abushagur A, Arsad N, Reaz M, Bakar A (2014) Advances in bio-tactile sensors for minimally invasive surgery using the fibre Bragg grating force sensor technique: a survey. *Sensors* 14(4):6633–6665
61. Correia R, Sinha R, Norris A, Korposh S, Talbot S, Hernandez F, Hayes-Gill B, Morgan S (2017) Optical fibre sensing at the interface between tissue and medical device. In: *International Conference on Biophotonics V. International Society for Optics and Photonics*, p 103400X
62. Wang DH-C, Blenman N, Maunder S, Patton V, Arkwright J (2013) An optical fiber Bragg grating force sensor for monitoring sub-bandage pressure during compression therapy. *Opt Express* 21(17):19799–19807
63. Su H, Zervas M, Furlong C, Fischer GS (2011) A miniature MRI-compatible fiber-optic force sensor utilizing Fabry-Pérot interferometer. In: *MEMS and Nanotechnology*, vol 4. Springer, pp 131–136
64. Su H, Zervas M, Cole GA, Furlong C, Fischer GS (2011) Real-time MRI-guided needle placement robot with integrated fiber optic force sensing. In: *2011 IEEE international conference on robotics and automation. IEEE*, pp 1583–1588
65. Liu X, Iordachita II, He X, Taylor RH, Kang JU (2012) Miniature fiber-optic force sensor based on low-coherence Fabry-Pérot interferometry for vitreoretinal microsurgery. *Biomed Opt Express* 3(5):1062–1076
66. Du Y, Yang Q, Huang J (2017) Soft prosthetic forefinger tactile sensing via a string of intact single mode optical fiber. *IEEE Sensors J* 17(22):7455–7459
67. Anwar Zawawi M, O’Keffe S, Lewis E (2013) Intensity-modulated fiber optic sensor for health monitoring applications: a comparative review. *Sens Rev* 33(1):57–67
68. Dziuda L, Skibniewski FW, Krej M, Lewandowski J (2012) Monitoring respiration and cardiac activity using fiber Bragg grating-based sensor. *IEEE Trans Biomed Eng* 59(7):1934–1942
69. Allsop TD, Carroll K, Lloyd G, Webb DJ, Miller M, Bennion I (2007) Application of long-period-grating sensors to respiratory plethysmography. *J Biomed Opt* 12(6):064003
70. Dziuda Ł (2015) Fiber-optic sensors for monitoring patient physiological parameters: a review of applicable technologies and relevance to use during magnetic resonance imaging procedures. *J Biomed Opt* 20(1):010901
71. Jia D, Chao J, Li S, Zhang H, Yan Y, Liu T, Sun Y (2017) A fiber Bragg grating sensor for radial artery pulse waveform measurement. *IEEE Trans Biomed Eng* 65(4):839–846
72. Sharath U, Sukreet R, Apoorva G, Asokan S (2013) Blood pressure evaluation using sphygmomanometry assisted by arterial pulse waveform detection by fiber Bragg grating pulse device. *J Biomed Opt* 18(6):067010
73. Mathew J, Semenova Y, Farrell G (2012) A miniature optical breathing sensor. *Biomed Opt Express* 3(12):3325–3331
74. Kang Y, Ruan H, Wang Y, Arregui F, Matias I, Claus R (2006) Nanostructured optical fibre sensors for breathing airflow monitoring. *Meas Sci Technol* 17(5):1207
75. Favero FC, Pruneri V, Villatoro J (2012) Microstructured optical fiber interferometric breathing sensor. *J Biomed Opt* 17(3):037006
76. Yoo WJ, Jang KW, Seo JK, Heo JY, Moon JS, Jun JH, Park J-Y, Lee B (2011) Development of optical fiber-based respiration sensor for noninvasive respiratory monitoring. *Opt Rev* 18(1):132–138
77. Charrett TO, James SW, Tatam RP (2012) Optical fibre laser velocimetry: a review. *Meas Sci Technol* 23(3):032001
78. Khotiantsev SN, Svirid V, Glebova L (1996) Laser Doppler velocimeter miniature differential probe for biomedical applications. In: *Biomedical systems and technologies. International Society for Optics and Photonics*, pp 158–165
79. Chahal R, Starecki F, Boussard-Plédel C, Doualan J-L, Michel K, Brilland L, Braud A, Camy P, Bureau B, Nazabal V (2016) Fiber evanescent wave spectroscopy based on IR fluorescent chalcogenide fibers. *Sensors Actuators B Chem* 229:209–216

80. Anne M-L, Keirse J, Nazabal V, Hyodo K, Inoue S, Boussard-Plédel C, Lhermite H, Charrier J, Yanakata K, Loreal O (2009) Chalcogenide glass optical waveguides for infrared biosensing. *Sensors* 9(9):7398–7411
81. Michel K, Bureau B, Boussard-Plédel C, Jouan T, Adam J, Staubmann K, Baumann T (2004) Monitoring of pollutant in waste water by infrared spectroscopy using chalcogenide glass optical fibers. *Sensors Actuators B Chem* 101(1–2):252–259
82. Le Coq D, Michel K, Keirse J, Boussard-Plédel C, Fonteneau G, Bureau B, Le Quéré J-M, Sire O, Lucas J (2002) Infrared glass fibers for in-situ sensing, chemical and biochemical reactions. *C R Chim* 5(12):907–913
83. Anne M-L, Le Lan C, Monbet V, Boussard-Plédel C, Ropert M, Sire O, Pouchard M, Jard C, Lucas J, Adam J-L (2009) Fiber evanescent wave spectroscopy using the mid-infrared provides useful fingerprints for metabolic profiling in humans. *J Biomed Opt* 14(5):054033
84. Wilhelm AA, Lucas P, DeRosa DL, Riley MR (2007) Biocompatibility of Te–As–Se glass fibers for cell-based bio-optic infrared sensors. *J Mater Res* 22(4):1098–1104
85. Leung A, Shankar PM, Mutharasan R (2007) A review of fiber-optic biosensors. *Sensors Actuators B Chem* 125(2):688–703
86. Siegmund H-U, Heiliger L, Van Lent B, Becker A (1998) Optical solid-phase biosensor based on polyionic layers labelled with fluorescent dyes. Google Patents
87. Flora K, Brennan JD (1999) Comparison of formats for the development of fiber-optic biosensors utilizing sol-gel derived materials entrapping fluorescently-labelled protein. *Analyst* 124(10):1455–1462
88. Tian Y, Wang W, Wu N, Zou X, Wang X (2011) Tapered optical fiber sensor for label-free detection of biomolecules. *Sensors* 11(4):3780–3790
89. Latifi H, Zibaii MI, Hosseini SM, Jorge P (2012) Nonadiabatic tapered optical fiber for biosensor applications. *Photonic Sensors* 2(4):340–356
90. Gupta RK, Periyakaruppan A, Meyyappan M, Koehne JE (2014) Label-free detection of C-reactive protein using a carbon nanofiber based biosensor. *Biosens Bioelectron* 59:112–119
91. Fan X, White IM, Shopova SI, Zhu H, Suter JD, Sun Y (2008) Sensitive optical biosensors for unlabeled targets: a review. *Anal Chim Acta* 620(1–2):8–26
92. Marques L, Hernandez F, James SW, Morgan S, Clark M, Tatam RP, Korposh S (2016) Highly sensitive optical fibre long period grating biosensor anchored with silica core gold shell nanoparticles. *Biosens Bioelectron* 75:222–231
93. Moreira L, Goncalves HM, Pereira L, Castro C, Jorge P, Gouveia C, Fernandes JR, Martins-Lopes P (2016) Label-free optical biosensor for direct complex DNA detection using *Vitis vinifera* L. *Sensors Actuators B Chem* 234:92–97
94. Chen X, Zhang L, Zhou K, Davies E, Sugden K, Bennion I, Hughes M, Hine A (2007) Real-time detection of DNA interactions with long-period fiber-grating-based biosensor. *Opt Lett* 32(17):2541–2543
95. Sozzi M, Coscelli E, Poli F, Cucinotta A, Selleri S, Corradini R, Marchelli R, Konstantaki M, Pissadakis S (2011) Long period grating-based fiber optic sensor for label-free DNA detection. In: 2011 International workshop on biophotonics. IEEE, pp 1–3
96. Chiavaioli F, Biswas P, Trono C, Jana S, Bandyopadhyay S, Basumallick N, Giannetti A, Tombelli S, Bera S, Mallick A (2015) Sol-gel-based titania-silica thin film overlay for long period fiber grating-based biosensors. *Anal Chem* 87(24):12024–12031
97. Biswas P, Chiavaioli F, Jana S, Basumallick N, Trono C, Giannetti A, Tombelli S, Mallick A, Baldini F, Bandyopadhyay S (2017) Design, fabrication and characterisation of silica-titania thin film coated over coupled long period fibre gratings: towards bio-sensing applications. *Sensors Actuators B Chem* 253:418–427
98. Bhatia V, Vengsarkar AM (1996) Optical fiber long-period grating sensors. *Opt Lett* 21(9):692–694
99. Homola J, Yee SS, Gauglitz G (1999) Surface plasmon resonance sensors. *Sensors Actuators B Chem* 54(1–2):3–15
100. Caucheteur C, Guo T, Albert J (2015) Review of plasmonic fiber optic biochemical sensors: improving the limit of detection. *Anal Bioanal Chem* 407(14):3883–3897
101. Lin H-Y, Tsao Y-C, Tsai W-H, Yang Y-W, Yan T-R, Sheu B-C (2007) Development and application of side-polished fiber immunosensor based on surface plasmon resonance for the detection of *Legionella pneumophila* with halogens light and 850 nm-LED. *Sens Actuators A Phys* 138(2):299–305

102. Slavik R, Homola J, Brynda E (2002) A miniature fiber optic surface plasmon resonance sensor for fast detection of staphylococcal enterotoxin B. *Biosens Bioelectron* 17 (6-7):591-595
103. Kanso M, Cuenot S, Louarn G (2008) Sensitivity of optical fiber sensor based on surface plasmon resonance: modeling and experiments. *Plasmonics* 3(2-3):49-57
104. Huang C-T, Jen C-P, Chao T-C, Wu W-T, Li W-Y, Chau L-K (2009) A novel design of grooved fibers for fiber-optic localized plasmon resonance biosensors. *Sensors* 9 (8):6456-6470
105. Wu W-T, Jen C-P, Tsao T-C, Shen W-C, Cheng C-W, Chen C-H, Tang J-L, Li W-Y, Chau L-K (2009) U-shaped fiber optics fabricated with a femtosecond laser and integrated into a localized plasmon resonance biosensor. In: 2009 symposium on design, test, integration & packaging of MEMS/MOEMS. IEEE, pp 127-131
106. Singh S, Gupta BD (2013) Fabrication and characterization of a surface plasmon resonance based fiber optic sensor using gel entrapment technique for the detection of low glucose concentration. *Sensors Actuators B Chem* 177:589-595
107. Ahn JH, Seong TY, Kim WM, Lee TS, Kim I, Lee K-S (2012) Fiber-optic waveguide coupled surface plasmon resonance sensor. *Opt Express* 20(19):21729-21738
108. Esteban Ó, Naranjo FB, Díaz-Herrera N, Valdueza-Felip S, Navarrete M-C, González-Cano A (2011) High-sensitive SPR sensing with Indium Nitride as a dielectric overlay of optical fibers. *Sensors Actuators B Chem* 158 (1):372-376
109. Navarrete M-C, Díaz-Herrera N, González-Cano A, Esteban Ó (2014) Surface plasmon resonance in the visible region in sensors based on tapered optical fibers. *Sensors Actuators B Chem* 190:881-885
110. Chang Y-J, Chen Y-C, Kuo H-L, Wei P-K (2006) Nanofiber optic sensor based on the excitation of surface plasmon wave near fiber tip. *J Biomed Opt* 11(1):014032
111. Wieduwilt T, Kirsch K, Dellith J, Willsch R, Bartelt H (2013) Optical fiber micro-taper with circular symmetric gold coating for sensor applications based on surface plasmon resonance. *Plasmonics* 8(2):545-554
112. Iga M, Seki A, Watanabe K (2004) Hetero-core structured fiber optic surface plasmon resonance sensor with silver film. *Sensors Actuators B Chem* 101(3):368-372
113. Takagi K, Sasaki H, Seki A, Watanabe K (2010) Surface plasmon resonances of a curved hetero-core optical fiber sensor. *Sens Actuators A Phys* 161(1-2):1-5
114. Wang P, Brambilla G, Ding M, Semenova Y, Wu Q, Farrell G (2011) High-sensitivity, evanescent field refractometric sensor based on a tapered, multimode fiber interference. *Opt Lett* 36(12):2233-2235
115. Sai V, Kundu T, Mukherji S (2009) Novel U-bent fiber optic probe for localized surface plasmon resonance based biosensor. *Biosens Bioelectron* 24(9):2804-2809
116. Gowri A, Sai V (2016) Development of LSPR based U-bent plastic optical fiber sensors. *Sensors Actuators B Chem* 230:536-543
117. He Y-J, Lo Y-L, Huang J-F (2006) Optical-fiber surface-plasmon-resonance sensor employing long-period fiber gratings in multiplexing. *JOSA B* 23(5):801-811
118. Schuster T, Herschel R, Neumann N, Schaffer CG (2011) Miniaturized long-period fiber grating assisted surface plasmon resonance sensor. *J Lightwave Technol* 30 (8):1003-1008
119. Nemova G, Kashyap R (2006) Fiber-Bragg-grating-assisted surface plasmon-polariton sensor. *Opt Lett* 31(14):2118-2120
120. Iadicco A, Cusano A, Campopiano S, Cutolo A, Giordano M (2005) Thinned fiber Bragg gratings as refractive index sensors. *IEEE Sensors J* 5(6):1288-1295
121. Albert J, Shao LY, Caucheteur C (2013) Tilted fiber Bragg grating sensors. *Laser Photonics Rev* 7(1):83-108
122. Shevchenko YY, Albert J (2007) Plasmon resonances in gold-coated tilted fiber Bragg gratings. *Opt Lett* 32(3):211-213
123. Caucheteur C, Voisin V, Albert J (2013) Polarized spectral combs probe optical fiber surface plasmons. *Opt Express* 21 (3):3055-3066
124. Bialiyayeu A, Bottomley A, Prezgot D, Ianoul A, Albert J (2012) Plasmon-enhanced refractometry using silver nanowire coatings on tilted fibre Bragg gratings. *Nanotechnology* 23(44):444012
125. Guo T, González-Vila Á, Loyez M, Caucheteur C (2017) Plasmonic optical fiber-grating immunosensing: a review. *Sensors* 17 (12):2732
126. Albert J, Lepinay S, Caucheteur C, DeRosa MC (2013) High resolution grating-assisted surface plasmon resonance fiber optic aptasensor. *Methods* 63(3):239-254

127. Hassani A, Skorobogatiy M (2007) Design criteria for microstructured-optical-fiber-based surface-plasmon-resonance sensors. *JOSA B* 24(6):1423–1429
128. Hautakorpi M, Mattinen M, Ludvigsen H (2008) Surface-plasmon-resonance sensor based on three-hole microstructured optical fiber. *Opt Express* 16(12):8427–8432
129. Nguyen H, Sidirolglou F, Collins S, Davis T, Roberts A, Baxter G (2013) A localized surface plasmon resonance-based optical fiber sensor with sub-wavelength apertures. *Appl Phys Lett* 103(19):193116
130. Consales M, Ricciardi A, Crescitelli A, Esposito E, Cutolo A, Cusano A (2012) Lab-on-fiber technology: toward multifunctional optical nanoprobos. *ACS Nano* 6(4):3163–3170
131. Jeong H-H, Lee S-K, Park J-H, Erdene N, Jeong D-H (2011) Fabrication of fiber-optic localized surface plasmon resonance sensor and its application to detect antibody-antigen reaction of interferon-gamma. *Opt Eng* 50(12):124405
132. Lin Y, Zou Y, Mo Y, Guo J, Lindquist RG (2010) E-beam patterned gold nanodot arrays on optical fiber tips for localized surface plasmon resonance biochemical sensing. *Sensors* 10(10):9397–9406
133. Lan X, Cheng B, Yang Q, Huang J, Wang H, Ma Y, Shi H, Xiao H (2014) Reflection based extraordinary optical transmission fiber optic probe for refractive index sensing. *Sensors Actuators B Chem* 193:95–99
134. Jasim I, Liu J, Yang Y, Qu C, Zhu C, Roman M, Huang J, Kinzel E, Almasri M (2019) Low-cost fabrication of functional plasmonic fiber-optic-based sensors using microsphere photolithography. In: *Fiber optic sensors and applications XVI*. International Society for Optics and Photonics, p 110000D
135. Schwalfenberg GK (2012) The alkaline diet: is there evidence that an alkaline pH diet benefits health? *J Environ Public Health* 2012:727630
136. Wolthuis R, McCrae D, Saaski E, Hartl J, Mitchell G (1992) Development of a medical fiber-optic pH sensor based on optical absorption. *IEEE Trans Biomed Eng* 39(5):531–537
137. Lin J (2000) Recent development and applications of optical and fiber-optic pH sensors. *TrAC Trends Anal Chem* 19(9):541–552
138. Gu B, Yin M-J, Zhang AP, Qian J-W, He S (2009) Low-cost high-performance fiber-optic pH sensor based on thin-core fiber modal interferometer. *Opt Express* 17(25):22296–22302
139. McCulloch S, Uttamchandani D (1997) Development of a fibre optic micro-optrode for intracellular pH measurements. *IEE Proceedings-Optoelectronics* 144(3):162–167
140. Goicoechea J, Zamarreño C, Matias I, Arregui F (2009) Utilization of white light interferometry in pH sensing applications by mean of the fabrication of nanostructured cavities. *Sensors Actuators B Chem* 138(2):613–618
141. Corres JM, Del Villar I, Matias IR, Arregui FJ (2007) Fiber-optic pH-sensors in long-period fiber gratings using electrostatic self-assembly. *Opt Lett* 32(1):29–31
142. Shao L-Y, Yin M-J, Tam H-Y, Albert J (2013) Fiber optic pH sensor with self-assembled polymer multilayer nanocoatings. *Sensors* 13(2):1425–1434
143. Corres JM, Matias IR, del Villar I, Arregui FJ (2007) Design of pH sensors in long-period fiber gratings using polymeric nanocoatings. *IEEE Sensors J* 7(3):455–463
144. Chu C-S, Lo Y-L, Sung T-W (2011) Review on recent developments of fluorescent oxygen and carbon dioxide optical fiber sensors. *Photonic Sensors* 1(3):234–250
145. Wolfbeis OS, Weis LJ, Leiner MJ, Ziegler WE (1988) Fiber-optic fluorosensor for oxygen and carbon dioxide. *Anal Chem* 60(19):2028–2030
146. Zhou H-C, Long JR, Yaghi OM (2012) Introduction to metal-organic frameworks. ACS Publications
147. Kreno LE, Leong K, Farha OK, Allendorf M, Van Duyen RP, Hupp JT (2011) Metal-organic framework materials as chemical sensors. *Chem Rev* 112(2):1105–1125
148. Kim K-J, Lu P, Culp JT, Ohodnicki PR (2018) Metal-organic framework thin film coated optical fiber sensors: a novel waveguide-based chemical sensing platform. *ACS sensors* 3(2):386–394
149. Hromadka J, Tokay B, Correia R, Morgan SP, Korposh S (2018) Carbon dioxide measurements using long period grating optical fibre sensor coated with metal organic framework HKUST-1. *Sensors Actuators B Chem* 255:2483–2494
150. Timmer B, Olthuis W, Van Den Berg A (2005) Ammonia sensors and their applications—a review. *Sensors Actuators B Chem* 107(2):666–677
151. Wolfbeis OS, Posch HE (1986) Fibre-optic fluorescing sensor for ammonia. *Anal Chim Acta* 185:321–327

152. Ibrahim S, Rahman N, Bakar MA, Girei S, Yaacob M, Ahmad H, Mahdi M (2015) Room temperature ammonia sensing using tapered multimode fiber coated with polyaniline nanofibers. *Opt Express* 23 (3):2837–2845
153. Fu H, Jiang Y, Ding J, Zhang J, Zhang M, Zhu Y, Li H (2018) Zinc oxide nanoparticle incorporated graphene oxide as sensing coating for interferometric optical microfiber for ammonia gas detection. *Sensors Actuators B Chem* 254:239–247
154. Tanguy NR, Thompson M, Yan N (2018) A review on advances in application of polyaniline for ammonia detection. *Sensors Actuators B Chem* 257:1044–1064
155. Wang T, Yasukochi W, Korposh S, James SW, Tatam RP, Lee S-W (2016) A long period grating optical fiber sensor with nano-assembled porphyrin layers for detecting ammonia gas. *Sensors Actuators B Chem* 228:573–580
156. Liu D, Han W, Mallik AK, Yuan J, Yu C, Farrell G, Semenova Y, Wu Q (2016) High sensitivity sol-gel silica coated optical fiber sensor for detection of ammonia in water. *Opt Express* 24(21):24179–24187
157. Kanawade R, Kumar A, Pawar D, Late D, Mondal S, Sinha RK (2019) Fiber optic Fabry–Perot interferometer sensor: an efficient and fast approach for ammonia gas sensing. *JOSA B* 36(3):684–689
158. Shirasu M, Touhara K (2011) The scent of disease: volatile organic compounds of the human body related to disease and disorder. *The Journal of Biochemistry* 150 (3):257–266
159. Pavlou AK, Magan N, Jones JM, Brown J, Klatter P, Turner AP (2004) Detection of Mycobacterium tuberculosis (TB) in vitro and in situ using an electronic nose in combination with a neural network system. *Biosens Bioelectron* 20(3):538–544
160. Voss A, Baier V, Reisch R, von Roda K, Elsner P, Ahlers H, Stein G (2005) Smelling renal dysfunction via electronic nose. *Ann Biomed Eng* 33(5):656–660
161. Dalton P, Gelperin A, Preti G (2004) Volatile metabolic monitoring of glycemic status in diabetes using electronic olfaction. *Diabetes Technol Ther* 6(4):534–544
162. Turner AP, Magan N (2004) Electronic noses and disease diagnostics. *Nat Rev Microbiol* 2 (2):161
163. Selyanchyn R, Korposh S, Yasukochi W, Lee S-W (2011) A preliminary test for skin gas assessment using a porphyrin based evanescent wave optical fiber sensor. *Sensors & Transducers* 125(2):54
164. Elosúa C, Matías I, Barriain C, Arregui F (2008) Detection of volatile organic compounds based on optical fibre using nanostructured films. *Int J Smart Sens Intell Syst* 1:123–136
165. Renganathan B, Sastikumar D, Srinivasan R, Ganesan A (2014) Nanocrystalline samarium oxide coated fiber optic gas sensor. *Mater Sci Eng B* 186:122–127
166. Hromadka J, James S, Davis F, Tatam RP, Crump D, Korposh S (2015) Detection of the volatile organic compounds emitted from paints using optical fibre long period grating modified with the mesoporous nanoscale coating. In: 24th international conference on optical fibre sensors. International Society for Optics and Photonics, p 96344K
167. Hernandez FU, Morgan SP, Hayes-Gill BR, Harvey D, Kinnear W, Norris A, Evans D, Hardman JG, Korposh S (2016) Characterization and use of a fiber optic sensor based on PAH/SiO₂ film for humidity sensing in ventilator care equipment. *IEEE Trans Biomed Eng* 63(9):1985–1992
168. Islam M, Ali M, Lai M-H, Lim K-S, Ahmad H (2014) Chronology of Fabry-Perot interferometer fiber-optic sensors and their applications: a review. *Sensors* 14(4):7451–7488
169. Ascorbe J, Corres J, Arregui F, Matias I (2017) Recent developments in fiber optics humidity sensors. *Sensors* 17(4):893
170. Konstantaki M, Pissadakis S, Pispas S, Madamopoulos N, Vainos NA (2006) Optical fiber long-period grating humidity sensor with poly (ethylene oxide)/cobalt chloride coating. *Appl Opt* 45(19):4567–4571
171. Alwis L, Sun T, Grattan K (2013) Optical fibre-based sensor technology for humidity and moisture measurement: review of recent progress. *Measurement* 46(10):4052–4074
172. Hernaez M, Zamarréno C, Melendi-Espina S, Bird L, Mayes A, Arregui F (2017) Optical fibre sensors using graphene-based materials: a review. *Sensors* 17(1):155
173. Zhao Y, X-G L, Zhou X, Y-N Z (2016) Review on the graphene based optical fiber chemical and biological sensors. *Sensors Actuators B Chem* 231:324–340
174. Li C, Yu X, Zhou W, Cui Y, Liu J, Fan S (2018) Ultrafast miniature fiber-tip Fabry–Perot humidity sensor with thin graphene oxide diaphragm. *Opt Lett* 43 (19):4719–4722
175. Jiang B, Bi Z, Hao Z, Yuan Q, Feng D, Zhou K, Zhang L, Gan X, Zhao J (2019)

- Graphene oxide-deposited tilted fiber grating for ultrafast humidity sensing and human breath monitoring. *Sensors Actuators B Chem* 293:336–341
176. Gomez D, Morgan SP, Hayes-Gill BR, Correia RG, Korposh S (2018) Polymeric optical fibre sensor coated by SiO₂ nanoparticles for humidity sensing in the skin microenvironment. *Sensors Actuators B Chem* 254:887–895
177. Tan W, Shi Z-Y, Smith S, Birnbaum D, Kopelman R (1992) Submicrometer intracellular chemical optical fiber sensors. *Science* 258 (5083):778–781
178. Vo-Dinh T (2002) Nanobiosensors: probing the sanctuary of individual living cells. *J Cell Biochem* 87(S39):154–161
179. Velasco-Garcia M (2009) Optical biosensors for probing at the cellular level: a review of recent progress and future prospects. In: *Seminars in cell & developmental biology*, vol 1. Elsevier, pp 27–33
180. Cullum BM, Griffin GD, Miller GH, Vo-Dinh T (2000) Intracellular measurements in mammary carcinoma cells using fiber-optic nanosensors. *Anal Biochem* 277 (1):25–32
181. Kasili P, Cullum B, Griffin G, Vo-Dinh T (2002) Nanosensor for in vivo measurement of the carcinogen benzo [a] pyrene in a single cell. *J Nanosci Nanotechnol* 2(6):653–658
182. Kasili PM, Song JM, Vo-Dinh T (2004) Optical sensor for the detection of caspase-9 activity in a single cell. *J Am Chem Soc* 126 (9):2799–2806
183. Yang Q, Wang H, Chen S, Lan X, Xiao H, Shi H, Ma Y (2015) Fiber-optic-based microprobe using hexagonal 1-in-6 fiber configuration for intracellular single-cell pH measurement. *Anal Chem* 87(14):7171–7179
184. Yang Q, Wang H, Lan X, Cheng B, Chen S, Shi H, Xiao H, Ma Y (2015) Reflection-mode micro-spherical fiber-optic probes for in vitro real-time and single-cell level pH sensing. *Sensors Actuators B Chem* 207:571–580
185. Vollmer F, Arnold S (2008) Whispering-gallery-mode biosensing: label-free detection down to single molecules. *Nat Methods* 5 (7):591
186. Whitesides GM (2006) The origins and the future of microfluidics. *Nature* 442 (7101):368
187. Psaltis D, Quake SR, Yang C (2006) Developing optofluidic technology through the fusion of microfluidics and optics. *Nature* 442(7101):381
188. Haque M, Lee KK, Ho S, Fernandes LA, Herman PR (2014) Chemical-assisted femtosecond laser writing of lab-in-fibers. *Lab Chip* 14(19):3817–3829
189. Yuan L (2017) Femtosecond laser micromachining of advanced fiber optic sensors and devices. All Dissertations. 1954. https://tigerprints.clemson.edu/all_dissertations/1954
190. Yuan L, Huang J, Lan X, Wang H, Jiang L, Xiao H (2014) All-in-fiber optofluidic sensor fabricated by femtosecond laser assisted chemical etching. *Opt Lett* 39(8):2358–2361
191. Haque M (2014) Chemical-assisted femtosecond laser writing of lab-in-fiber sensors. University of Toronto (Canada)
192. Wang B, Mies E (2007) Advanced topics on fusion splicing of specialty fibers and devices. In: *Passive components and fiber-based devices IV*. International Society for Optics and Photonics, p 678130
193. Xiao L, Demokan M, Jin W, Wang Y, Zhao C-L (2007) Fusion splicing photonic crystal fibers and conventional single-mode fibers: microhole collapse effect. *J Lightwave Technol* 25(11):3563–3574
194. Zhang S, Zhang W, Gao S, Geng P, Xue X (2012) Fiber-optic bending vector sensor based on Mach-Zehnder interferometer exploiting lateral-offset and up-taper. *Opt Lett* 37(21):4480–4482
195. Yin G, Lou S, Zou H (2013) Refractive index sensor with asymmetrical fiber Mach-Zehnder interferometer based on concatenating single-mode abrupt taper and core-offset section. *Opt Laser Technol* 45:294–300
196. Huang R, Ni K, Ma Q, Wu X (2016) Refractometer based on a tapered Mach-Zehnder interferometer with Peanut-Shape structure. *Opt Lasers Eng* 83:80–82
197. Tian K, Zhang M, Farrell G, Wang R, Lewis E, Wang P (2018) Highly sensitive strain sensor based on composite interference established within S-tapered multimode fiber structure. *Opt Express* 26(26):33982–33992
198. Felipe A, Espíndola G, Kalinowski HJ, Lima JA, Paterno AS (2012) Stepwise fabrication of arbitrary fiber optic tapers. *Opt Express* 20 (18):19893–19904
199. Liu Z-H, Lei J-J, Zhang Y, Zhang Y-X, Yang X-H, Zhang J-Z, Yang Y, Yuan L-B (2018) Microparticle collection for water purification based on laser-induced convection. *Chinese Physics B* 27(5):054209
200. Tong L, Gattass RR, Ashcom JB, He S, Lou J, Shen M, Maxwell I, Mazur E (2003)

- Subwavelength-diameter silica wires for low-loss optical wave guiding. *Nature* 426 (6968):816
201. Liu Y, Meng C, Zhang AP, Xiao Y, Yu H, Tong L (2011) Compact microfiber Bragg gratings with high-index contrast. *Opt Lett* 36(16):3115–3117
 202. Lu P, Men L, Sooley K, Chen Q (2009) Tapered fiber Mach-Zehnder interferometer for simultaneous measurement of refractive index and temperature. *Appl Phys Lett* 94 (13):131110
 203. Tian Z, Yam SS-H, Barnes J, Bock W, Greig P, Fraser JM, Looock H-P, Oleschuk RD (2008) Refractive index sensing with Mach-Zehnder interferometer based on concatenating two single-mode fiber tapers. *IEEE Photon Technol Lett* 20(8):626–628
 204. Tien C-L, Chen H-W, Liu W-F, Jyu S-S, Lin S-W, Lin Y-S (2008) Hydrogen sensor based on side-polished fiber Bragg gratings coated with thin palladium film. *Thin Solid Films* 516(16):5360–5363
 205. Jang HS, Park KN, Kim JP, Sim SJ, Kwon OJ, Han Y-G, Lee KS (2009) Sensitive DNA biosensor based on a long-period grating formed on the side-polished fiber surface. *Opt Express* 17(5):3855–3860
 206. Luo Y, Wei Q, Ma Y, Lu H, Yu J, Tang J, Yu J, Fang J, Zhang J, Chen Z (2015) Side-polished-fiber based optical coupler assisted with a fused nano silica film. *Appl Opt* 54 (7):1598–1605
 207. Khan M, Kang S-W (2014) A high sensitivity and wide dynamic range fiber-optic sensor for low-concentration VOC gas detection. *Sensors* 14(12):23321–23336
 208. Chin LC, Whelan WM, Vitkin IA (2010) Optical fiber sensors for biomedical applications. In: *Optical-thermal response of laser-irradiated tissue*. Springer, pp 661–712
 209. Bae H, Zhang X, Liu H, Yu M (2010) Miniature surface-mountable Fabry-Perot pressure sensor constructed with a 45 angled fiber. *Opt Lett* 35(10):1701–1703
 210. Maiman TH (1960) Stimulated optical radiation in ruby. *A Century of Nature*, edited by Laura Garwin and Tim Lincoln, Chicago: University of Chicago Press, 2010, pp 113–114. <https://doi.org/10.7208/9780226284163-019>
 211. Osellame R, Cerullo G, Ramponi R (2012) *Femtosecond laser micromachining: photonic and microfluidic devices in transparent materials*, vol 123. Springer Science & Business Media
 212. Davis KM, Miura K, Sugimoto N, Hirao K (1996) Writing waveguides in glass with a femtosecond laser. *Opt Lett* 21 (21):1729–1731
 213. Wang Q, Wang D, Zhang H (2019) Fiber Bragg grating with a waveguide fabricated in no-core fiber and multimode fiber. *Opt Lett* 44(11):2693–2696
 214. Liu J, Yuan L, Lei J, Zhu W, Cheng B, Zhang Q, Song Y, Chen C, Xiao H (2017) Micro-cantilever-based fiber optic hydrophone fabricated by a femtosecond laser. *Opt Lett* 42(13):2459–2462
 215. Gamaly EG, Juodkazis S, Nishimura K, Misawa H, Luther-Davies B, Hallo L, Nicolai P, Tikhonchuk VT (2006) Laser-matter interaction in the bulk of a transparent solid: confined microexplosion and void formation. *Phys Rev B* 73(21):214101
 216. Taylor RS, Hnatovsky C, Simova E, Rayner DM, Bhardwaj V, Corkum PB (2003) Femtosecond laser fabrication of nanostructures in silica glass. *Opt Lett* 28(12):1043–1045
 217. Zhou P, Liao C, Li Z, Liu S, Wang Y (2019) In-fiber cascaded FPI fabricated by chemical-assisted femtosecond laser micromachining for micro-fluidic sensing applications. *J Lightwave Technol* 37(13):3214–3221
 218. Liu Y, Qu S, Li Y (2013) Single microchannel high-temperature fiber sensor by femtosecond laser-induced water breakdown. *Opt Lett* 38(3):335–337